TESTING AN ALGORITHM TO RAPIDLY DETERMINE EARTHQUAKE FAULT PARAMETERS FROM AFTERSHOCK LOCATIONS

Undergraduate Senior Thesis by

Kevin Kwong

In Partial Fulfillment of the Requirements
for the Degree of

Bachelor of Science in Geology

Undergraduate Advisor:

Dr. Jascha Polet

California State Polytechnic University, Pomona

Pomona, California

2011

(Defended May 26, 2011)

Acknowledgements

I would like to express my deepest gratitude to my advisor, Dr. Jascha Polet, who provided me excellent guidance and motivation for my research. Dr. Polet introduced me to geophysics and influenced me to pursue graduate school. Her support made this possible and as a result I am proud and happy about the academic decisions and research endeavors I have made.

I would like to also thank Dr. Jeff Marshall and Dr. Jon Nourse who also supported my graduate school aspirations and have written and submitted many letters of recommendations on my behalf.

Abstract

Aftershock locations may be used to determine reliable estimates of first-order earthquake rupture parameters more rapidly than may be obtained from full seismic waveform or geodetic inversions and field mapping. Because the spatial distribution of aftershocks for an earthquake sequence has a close empirical relation to its mainshock rupture extent, the epicentral locations of aftershocks can be used to delineate the entire mainshock rupture zone and to determine first-order parameters such as rupture length and orientation. An important goal of this research is to determine how early in an aftershock sequence we can reliably and accurately determine these rupture parameters. To this end we test an algorithm we developed for rapid estimation of these parameters in a near real-time environment. The results of this algorithm may provide useful information to help quickly assess the impact (damage and fatalities) of large global earthquakes when incorporated in a global earthquake analysis system, such as implemented by the US Geological Survey National Earthquake Information Center. Required input parameters to this algorithm are limited to an earthquake catalog starting with the mainshock time and other fixed input parameters. Aftershock events are projected onto straight lines centered on the mainshock epicenter with a fixed incremental azimuth. Subsequently, a best fitting strike and rupture length for the mainshock fault are determined on the basis of this aftershock distribution. We tested and compared our results to selected earthquakes in the Next Generation Attenuation Database. We then also tested earthquakes from a list of recent destructive earthquakes and compared our results to finite rupture models from full inversions. We show by applying the algorithm to these two sets of earthquakes that we can determine reliable first-order rupture parameters as early as 30 minutes after the mainshock occurrence using early aftershock locations.

Table of Contents

Acknowledgments i
Abstract ii

Introduction 1
Motivation 2
Methodology 3
Input Parameters 3
Algorithm Steps 4
Results 8
Working with the Next Generation Attenuation Database 8
Recent Earthquakes Resulting in Large Fatalities 16
M≥9 Megathrust Earthquake Ruptures 17
Non Elongated Rupture Planes 17
Well Constrained Events 18
Accessing the Effectiveness of Our Algorithm 25
Discussing Algorithm Improvement 28
Conclusions 28
References 30

Appendix A: Detailed Results for the 2010 Canterbury, New Zealand Earthquake 32
Appendix B: Rupture Parameters of Recent Destructive Earthquakes 34

List of Illustrations and Tables

Table 1.1: Source parameters of earthquakes used in our study (from the NGA database) **5**
Table 1.2: Source parameters of destructive earthquakes used in our study **5**
Figure 1.1: Algorithm Steps Applied to the 1999 Mw 7.1 Strike-Slip Hector Mine, California earthquake **6**
Figure 1.2: Algorithm Steps Applied to the 1999 Mw 7.1 Strike-Slip Hector Mine, California earthquake (Cont) **7**
Figure 2: Results for the 1999 Mw 7.1 Duzce, Turkey earthquake **9**
Figure 3: Results for the 1994 Mw 6.7 Northridge, California earthquake **10**
Figure 4: Results for the 1994 Mw 5.9 Double Springs, Nevada earthquake **11**
Table 2: Calculated results using largest bin method compared to NGA results **12**
Table 3: Calculated results using minimum length method compared to NGA results **13**
Figure 5: Largest bin method results vs. NGA results **14**
Figure 6: Minimum length method results vs. NGA results **14**
Figure 7: Results for the 2011 Mw 9.0 Tohoku, Japan earthquake **19**
Figure 8: Results for the 2004 Mw 9.1 Indian Ocean earthquake **20**
Figure 9: Results for the 2009 Mw 7.6 Southern Sumatra earthquake **21**
Figure 10: Results for the 2001 Mw 7.7 Gujarat India earthquake **22**
Figure 11: Results for the 2008 Mw 7.9 Eastern Sichuan, China earthquake **23**
Figure 12: Results for the 2010 Mw 7.0 Haiti earthquake **24**
Figure 13: Percentages of successfully determined rupture parameters vs. time **25**
Figure 14: Calculated rupture parameters vs. rupture parameters from full inversions **27**

In Appendices

Figure 15: Detailed results for the 2010 Mw 7.0 Canterbury, New Zealand earthquake **33**
Table 4: Calculated rupture parameters and reliable rupture parameters **34**

Introduction

Aftershocks are known to be smaller magnitude events that follow a larger magnitude mainshock event. The occurrences of aftershocks tend to follow certain empirical characteristics. The first empirical study that formalized the rate of aftershock occurrence was made by Omori (1894) for the Mino Owari (Nobi) Japan earthquake sequence. His observations for that earthquake sequence led him to postulate that the frequency of aftershock earthquakes dies off hyperbolically after the mainshock which is now called Omori's Law. Omori showed that n(t) being the rate of aftershocks at time t, where K and c are parameters , that Omori's law can be expressed as:

$$n(t) = \frac{K}{c+t}$$

Another empirical characteristic of aftershocks is that the area in which they occur gives a good estimate of the mainshock fault rupture area. The first to associate the location of aftershocks with the mainshock fault rupture area was Richter (1955). The 1952 Kern County, California earthquake was an example where the first portable seismometers were installed in the field within hours of the mainshock in hopes of recording aftershock events. The seismometers deployed in the vicinity of the mainshock epicentral region revealed information that aftershocks occurring in a short time after the mainshock were distributed over a roughly rectangular area giving a good estimate of the mainshock fault area as postulated by Richter. Being able to locate and study the spatial distribution of aftershocks has been very important in providing useful information about the mainshock event and an estimate of the mainshock fault rupture area.

Another empirical observation about aftershocks is that its area grows exponentially with mainshock magnitude (Utsu and Seki , 1955). They formulated an empirical relation that recognizes that the aftershock area in km^2 as S for a mainshock magnitude of M can be expressed in a simplified equation as:

$$\log S = M - 3.9$$

Also a similar equation recognizes the relationship between magnitude (M) and fault length (L) as:

$$\log L = .5M - 1.8$$

These empirical relationships and characteristics about the spatial distribution of aftershocks provide the main background for our study. We want to use the initial aftershock distribution for large earthquakes too see how well (and how fast) we can rapidly determine the rupture extent for large earthquakes.

Motivation

In the event of a significant earthquake, seismic data are collected and analyzed to aid in earthquake hazard mitigation. The National Earthquake Information Center (NEIC) puts near real time seismology into work by rapidly locating destructive earthquakes worldwide and determining their size and provide this information to the public. The rapid availability of a worldwide earthquake catalog provides an opportunity to look at earthquakes that occur immediately after a large mainshock event. We want to investigate how early we can determine the rupture extent of a large earthquake and in what direction it propagated, by using aftershock locations determined in near real-time. Being able to rapidly access the mainshock rupture with the initial distribution of aftershocks within a few hours after the mainshock occurrence, a more rapid assessment of earthquake impact can potentially be made. Determining source parameters of large earthquakes such as its rupture extent commonly involves methods such as full seismic waveform and/or geodetic inversions, and field mapping after the mainshock event. The former methods require complex computational techniques that involve looking at seismic and geodetic data. The later method can involve extensive airborne and on land field mapping in addition to surveying. However, all these methods are time consuming when trying to determine reliable results. In our study, we want to use a consistent method that will use the initial distribution of aftershocks to rapidly estimate fault rupture parameters.

Our method hopes to constrain earthquake rupture length and fault orientation for any particular large mainshock event. To calculate these rupture parameters quickly, we test an automatic algorithm that uses aftershock locations in a near real-time seismology environment. If we find that our algorithm does determine accurate earthquake rupture parameters, it is important to test at what consistent time period after the mainshock we can use our algorithm to determine reliable rupture parameters. To test our algorithm effectively, we examine a variety of large historic earthquakes that are mostly magnitude 6.5 or higher. If our method in using initial aftershock distributions to rapidly estimate fault rupture extent is reliable, the improvement of near real-time

determination of aftershock locations will be important to help rapidly constrain mainshock source parameters. By having a reliable automatic algorithm that rapidly determines mainshock fault geometry and rupture direction, it can provide early useful information to earthquake hazard assessment systems such as the Prompt Assessment of Global Earthquakes for Response (PAGER) at the US Geological Survey National Earthquake Information Center (Earle et al., 2009).

Methodology

We are testing an automatic algorithm developed to estimate fault rupture extent (e.g. fault length and strike) of large earthquakes using aftershock locations. This algorithm produces best fitting rupture parameters depending on the aftershocks located within a certain time after the mainshock. The algorithm will also determine whether the mainshock rupture fits the criteria of being unilateral (rupture in one direction on the fault) or bilateral (rupture in two directions on the fault).

Our algorithm was tested using a number of recent events of the last two decades. We first used earthquakes from the Next Generation Attenuation Relationships (NGA) database that contains source parameters of the mainshock. We then tested a number of recent large earthquakes over the last 10 years that resulted in fatalities of over 1,000 and compared our results to source parameters determined from full inversions (See tables 1.1 and 1.2 of the list of earthquakes with their source parameters we used in our study). The NGA rupture parameters were determined using a consistent method and gives us a consistent source to compare our results to. However, based on a quick review of the literature on the NGA earthquakes, we consider that a comparison with results from more recent earthquakes obtained from full waveform inversions may provide a more accurate picture of the reliability of the algorithm.

Input Parameters

The algorithm requires some input parameters such as the aftershock epicenters. We gather information about aftershock locations using an earthquake catalog primarily from the National Earthquake Information Center (NEIC) using the NEIC Earthquake Search interface at the U.S. Geological Survey Earthquake Hazards Program website. An earthquake catalog starting with the mainshock event is used as input parameters.

Algorithm Steps

The algorithm will compute the following steps for all earthquakes tested in this study. We will provide illustrations to these steps for the 1999 Mw 7.1 strike-slip Hector Mine earthquake in Southern California as an example (see Figure 1).

- The algorithm will first use the initial magnitude of the mainshock to determine an approximate fault length using the Wells and Coppersmith scaling relationships for the purpose of selecting an appropriate geographic area.
- The fault length selected will determine the geographic area as a box that will have a width and height of 4 times the fault length.
- If the algorithm determines a fault length twice this size then a new analysis will repeat the calculation for a geographic box twice the initial size.
- The algorithm will plot the aftershocks on a geographic map for a specified parameter of time since the mainshock.
- The algorithm determines what earthquakes plotted are true "aftershocks" and what are background seismicity and triggered events. Earthquakes that are considered true aftershocks are the presence of 5% of all events within 0.4° distance from its epicenter for the global NEIC catalog.
- Straight lines are projected through the mainshock epicenter with a fixed 10° incremental azimuth starting at 0° to 180°.
- Aftershock epicenters are projected perpendicularly to each of the incremental lines through the mainshock epicenter.
- The length of each of the projected aftershock distribution lines is determined by stepping away from the epicenter in steps of 5 km until 90% of aftershocks are contained.
- The fault strike is then determined by selecting the azimuth of the line perpendicular to the most concentrated distribution, which may be defined in two possible ways:
    1. The shortest projected distribution length (**the minimum length method**)

       or

    2. The distribution with the highest peak value (**the largest bin method**)

- The assessment of the nature of the rupture (bilateral or unilateral) is based on the location of the epicenter relative to the determined rupture extent. When more than 75% of the rupture length estimate is located on one side of the epicenter, the rupture is categorized as unilateral.

Table 1.1: Source parameters of earthquakes used in our study (from the NGA database)

Event ID	Date	Origin Time (UTC)	Region	Location Lat./Long.	Mw	Faulting Type	Fault Length (km)	Strike ((°)Azimuth)
MA	6/20/1990	0:30:09	Manjil, Iran	36.81ºN,49.35ºE	7.4	Strike Slip	71.6	112
GR	12/21/1990	6:57:45	Griva, Greece	40.96ºN,22.37ºE	6.1	Normal	17.5	54
ER	3/13/1992	17:18:46	Erzincan, Turkey	39.71ºN, 39.58ºE	6.7	Strike Slip	29.0	122
CM	4/25/1992	18: 6:11	Cape Mendocino, California	40.33ºN,-124.22ºE	7.0	Reverse	20.0	170
DS	9/12/1994	12:23:47	Double Springs, Nevada	38.82ºN,-199.63ºE	5.9	Strike Slip	10.0	21
NO	1/17/1994	12:31	Northridge, Southern California	34.20ºN, -188.55ºE	6.7	Reverse	18.0	122
KJ	1/16/1995	20:46:52	Kobe , Japan	34.58ºN, 135.01ºE	6.9	Strike Slip	60.0	50
KG	5/13/1995	8:47:20	Kozani, Greece	40.15ºN,21.67ºE	6.4	Normal	27.0	73
DI	10/1/1995	15:57	Dinar, Turkey	38.06ºN,30.15ºE	6.4	Normal	12.6	130
KO	8/17/1999	0:01:39	Kocaeli, Turkey	40.72ºN,29.99ºE	7.5	Strike Slip	137.5	92
CC	9/20/1999	17:47	Chi Chi, Taiwan	28.86ºN,120.79ºE	7.6	Reverse	88.0	5
HE	10/16/1999	9:46:45	Hector Mine, Southern California	34.57ºN,-116.29ºE	7.1	Strike Slip	69.0	151
DU	11/12/1999	16:57	Duzce, Turkey	40.77ºN,31.18ºE	7.1	Strike Slip	46.8	85
NM	10/23/2002	11:27:18	Nenana Mountain, Alaska	63.51ºN,-148.11ºE	6.7	Strike Slip	30.0	83

Table 1.2: Source parameters of destructive earthquakes used in our study with number of resulting fatalities (from USGS)

Event ID	Date	Origin Time (UTC)	Region	Location Lat. , Long.	Mw	Faulting Type	Fault Length Range (km)	Sources	Strike ((°)Azimuth)	Sources	Fatalities
TO	3/11/2011	14:46:23	Tōhoku, Japan	38.322°N, 142.369°E	9.0	Reverse	(250-300)	Ji et al. 2011	21	Wei et al, 2011	28,050
YU	4/13/2010	23:49:38	Southern Qinghai, China	33.224°N, 96.666°E	6.9	Strike-Slip	(30-65)	Chen et al. 2010, Zhang et al. 2010	130	Chen et al, 2010	2,968
HA	1/12/2010	21:53:10	Port-au-Prince, Haiti	18.443°N, 72.571°W	7.0	Strike-Slip	(30-35)	Hayes 2010, Sladen 2010	84	Gavin Hayes, 2010	222,570
SS	9/30/2009	10:16:09	Southern Sumatra, Indonesia	0.725°S, 99.856°E	7.6	Reverse	(20-35)	Hutko et al. 2009, Sladen 2009	71.3	Gavin Hayes, 2009	1,117
ES	5/12/2008	6:28:01	Eastern Sichuan, China	30.986°N, 103.364°E	7.9	Reverse	(210-290)	Ji et al. 2008, Zhang et al. 2008	49	Ji and Hayes, 2008	87,587
PA	10/8/2005	3:50:40	Kashmir, Pakistan	34.493°N, 73.629°E	7.6	Reverse	(65-90)	Chen Ji , 2005	153	Ji, 2005	86,000
NI	3/28/2005	16:09:36	Northern Sumatra, Indonesia	2.074°N, 97.013°E	8.6	Reverse	(330-425)	Ji et al. 2005, Borges et al, 2005	150	Borges et al, 2005	1,313
IO	12/26/2004	0:58:53	Indian Ocean	3.316°N, 95.854°E	9.1	Reverse	(1200-1600)	Huang et al. 2010, Lay et al. 2005	149	Tanioka et al, 2005	227,898
AL	5/21/2003	18:44:19	Northern Algeria	36.90°N, 3.71°E	6.8	Reverse	(54-65)	Meghraoui et al. 2004, Ayadi et al. 2008	54	Semmane et al, 2005	2,266
GU	1/26/2001	3:16:40	Gujarat, India	23.41°N, 70.23°E	7.7	Reverse	(40-60)	Mandal and Horton 2006	78	Negishi et al, 2002	20,023

Figure 1.1: Algorithm Steps Applied to the 1999 Mw 7.1 Strike-Slip Hector Mine, California Earthquake

A.

Outlier Removal

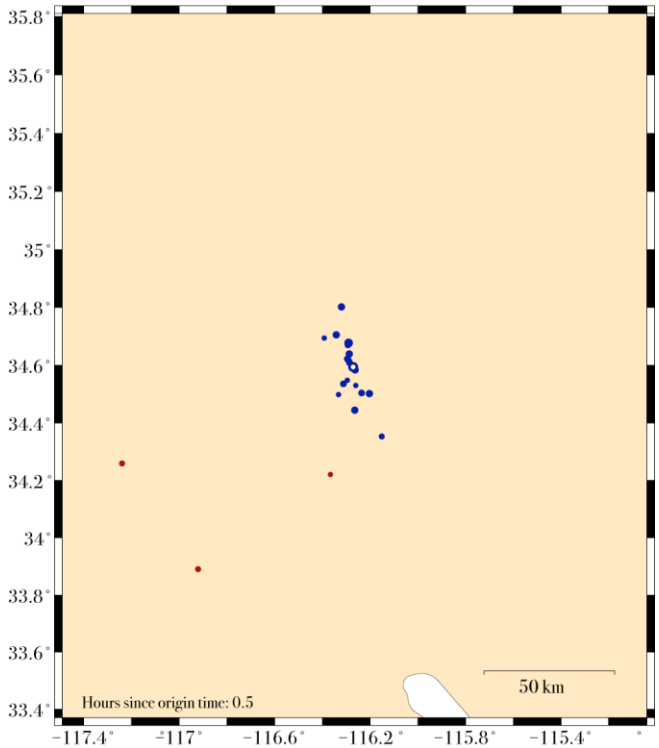

Figure 1A: *A map of the geographical region analyzed for the Hector Mine earthquake of 1999, using the standard (nonrelocated) SCSN earthquake catalog. Blue events were classified as "aftershocks" by the algorithm, which considers as outliers (in red) those earthquakes that have fewer than 5% of the total number of events within 0.2° distance of its epicenter.*

B.

Projection of Aftershock Epicenters

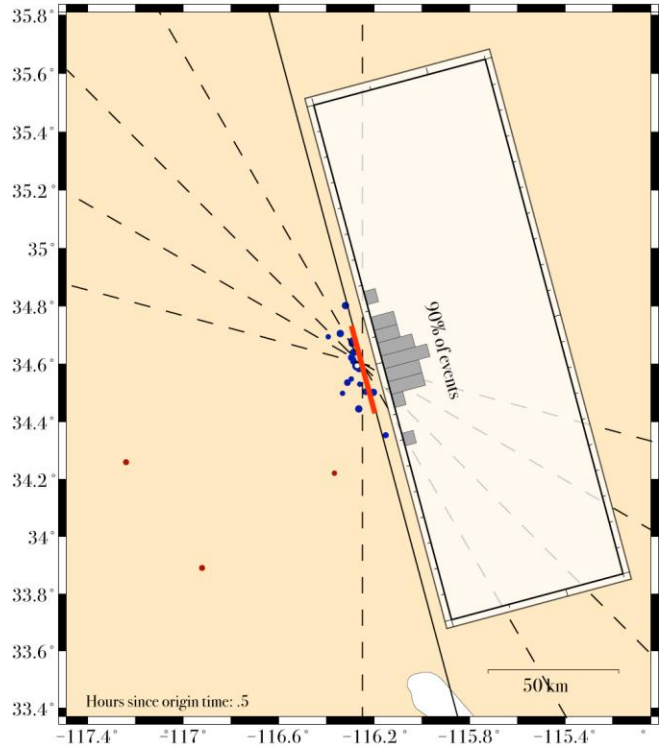

Figure 1B: *The aftershocks are projected onto straight lines centered on the mainshock epicenters, separated by 15° in azimuth (not all lines are shown in this plot for clarity). The projected aftershocks distributions are then binned in histograms with 5 km distance bins starting from the mainshock epicenter. The length of the projected distribution is determined by stepping outwards by 5 km steps, until 90% of the aftershocks are contained.*

C.

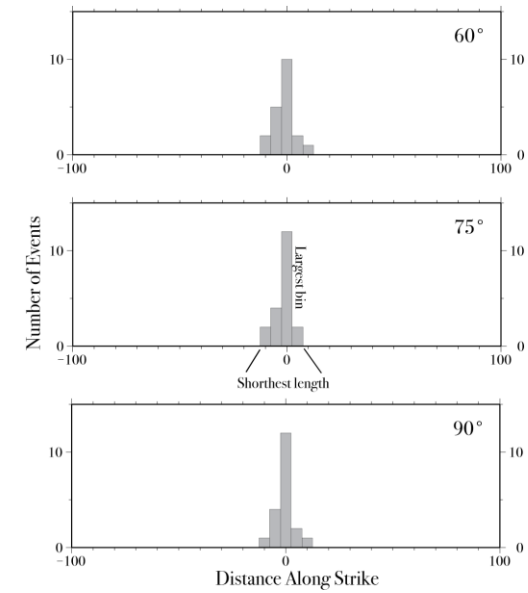

Figure 1C: *The projected aftershock distributions for three different azimuths. For this earthquake, the azimuth with the shortest projected distribution length is 75° and two azimuths have the bin with the largest numbers of events: 75° and 90°.*

Figure 1.2: Algorithm Steps Applied to the 1999 Mw 7.1 Strike-Slip Hector Mine, California Earthquake Cont.

D.

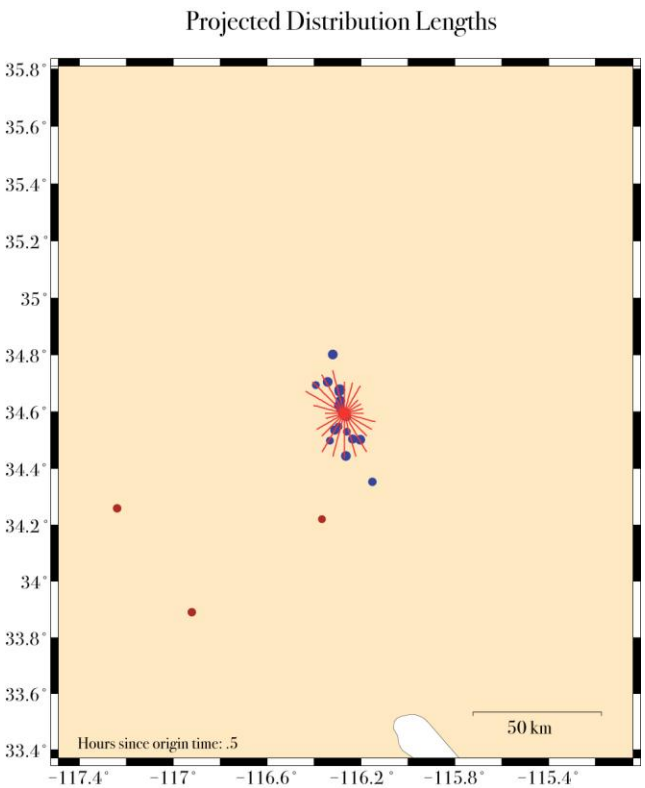

Figure 1.2D: *The red lines show the projected aftershock distribution lengths determined for the complete range of azimuths.*

E.

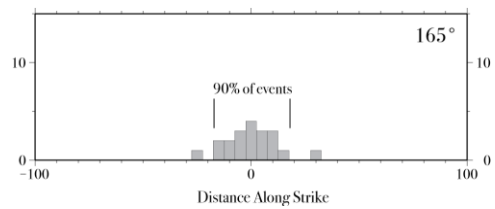

Figure 1.2E: *The aftershock distribution for the azimuth 90° away from the projected distribution with the shortest length. The azimuth of this line provides an estimate of the fault strike (165° from North). The Global CMT strike for the Hector Mine earthquake was determined to be 336° or 156°. The distribution length, calculated by stepping outwards from the epicenter with 5 km steps until 90% of aftershocks are contained within the bounds of the interval, is determined to be 35 km and provides an estimate of rupture length.*

F.

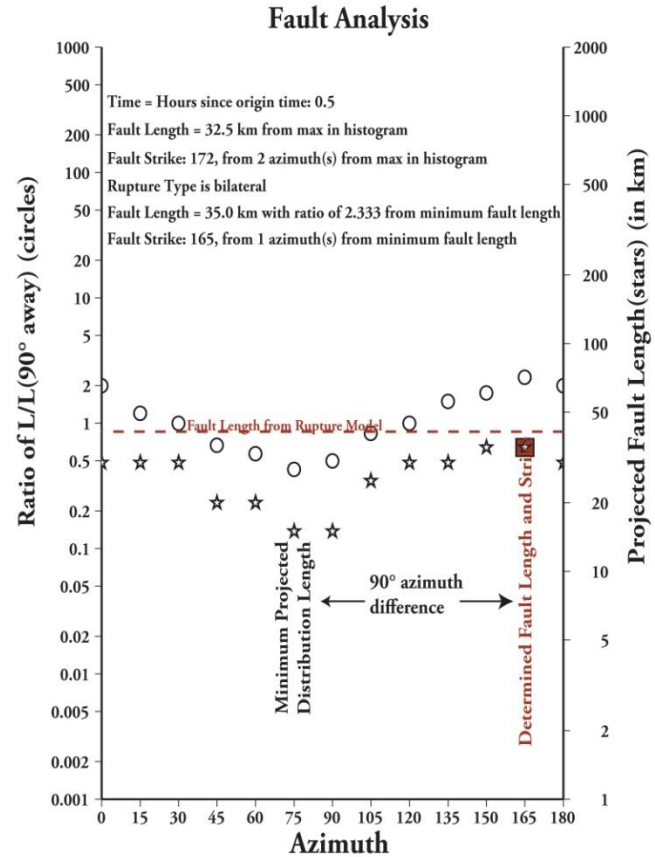

Figure 1.2F: *A summary of results for all azimuths, showing rupture lengths determined using the two different approaches. The ratio between the shortest distribution length and the length at an azimuth 90° away from this length determines how elongated the fault is, with better strike estimates determined for more elongated faults.*

Results

Working with the Next Generation Attenuation Database

The Next Generation Attenuation Relationships (NGA) database is an update and extension to the Peer Strong Motion Database and contains information on parameters for determined earthquake fault rupture length and orientation. Using the NGA database gives us a singular objective source that we can compare our calculated results with. We picked mainshock events in the database that were recent (events after 1990) and contained the mainshock source parameters needed as input data in our algorithm.

A total of 14 mainshock events were picked in the NGA database and we applied our algorithm to these events using a fixed 10º incremental azimuth in our aftershock distribution length projections. We show examples of our algorithm results of a well constrained event: the 1999 Mw 7.1 Duzce, Turkey earthquake, a moderately constrained event: the 1994 Mw 6.7 Northridge, California earthquake and a poorly constrained event: the 1994 Mw 5.9 Double Springs, Nevada earthquake (see Figures 2, 3, and 4). We show rupture parameter results of these events using aftershocks that occurred within 1 hour after the mainshock. Fault analyses of these earthquakes are shown for the full range of azimuths showing the rupture lengths determined using both of our methods. The red star indicates determined fault length and strike 90° from the minimum projected aftershock distribution length. The gray straight lines indicate rupture parameter results from the NGA database (See Figures 2a, 3a and 4a).

We also show map figures of the projected aftershock distribution lengths determined for a complete range of azimuths. Highlighted green line indicates the determined fault length and strike that is 90° from the minimum projected aftershock distribution length (see Figures 2b, 3b and 4b). We further analyze how constrained these three events are by showing our fault rupture length and strike results plotted against time up to 5 hours. The red line indicates the NGA results (see Figures 2c, 2d, 3c, 3d, 4c, 4d).

Our results indicate that in general using the minimum length method was the more reliable method of determining fault strikes as compared to the NGA results. However, we see that using the largest bin method worked better for determining fault length for the Northridge earthquake.

Figure 2: Results for the 1999 Mw 7.1 Duzce, Turkey earthquake

A. Fault analysis results for a full range of azimuths of 10° increments: Circles show the ratio of how elongated the fault is, Red stars show the projected fault lengths, gray lines indicate NGA results.

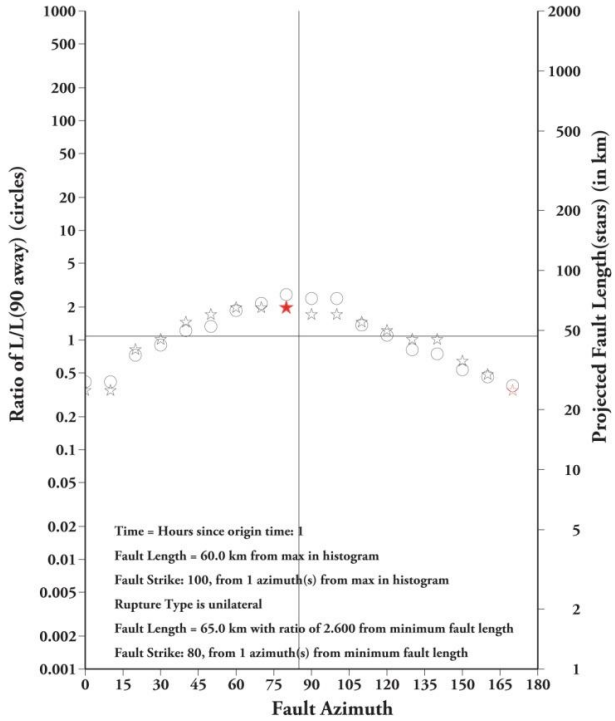

B. Map shows plotted aftershocks and red lines show projected fault lengths for a full range of azimuths of 10° increments, green line show determined fault length.

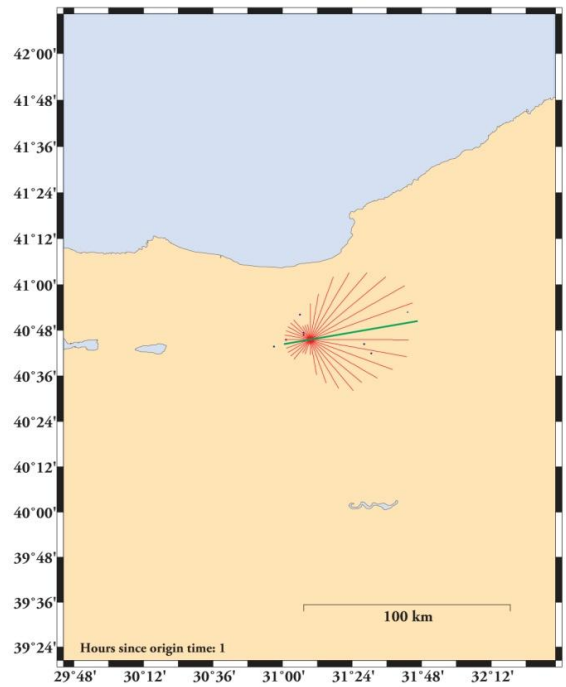

C. Fault length results vs. time since mainshock. Green circles show results from min length method and blue squares show results from largest bin method. Red line shows NGA results with ±10 km boundaries.

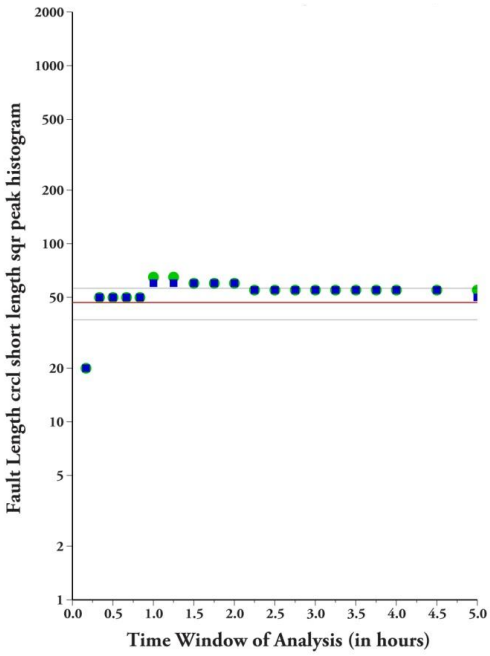

D. Fault azimuth results vs. time since mainshock. Green circles show results from min length method and blue squares show results from largest bin method. Red line shows NGA results with ± 15° boundaries.

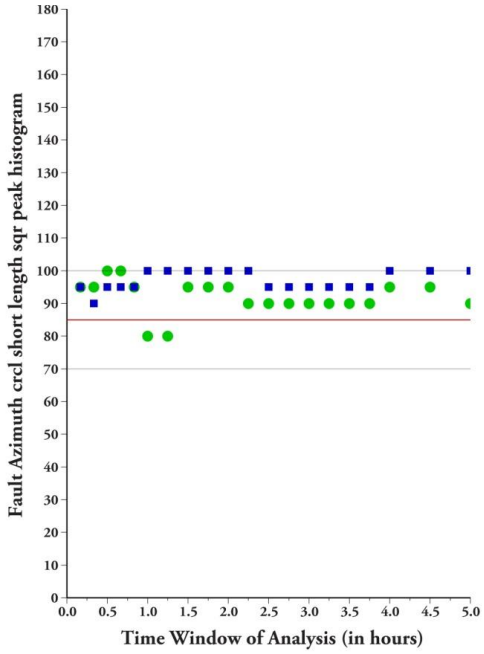

Figure 3: Results for the 1994 Mw 6.7 Northridge, California earthquake
(Captions for figures similar to Figure 2)

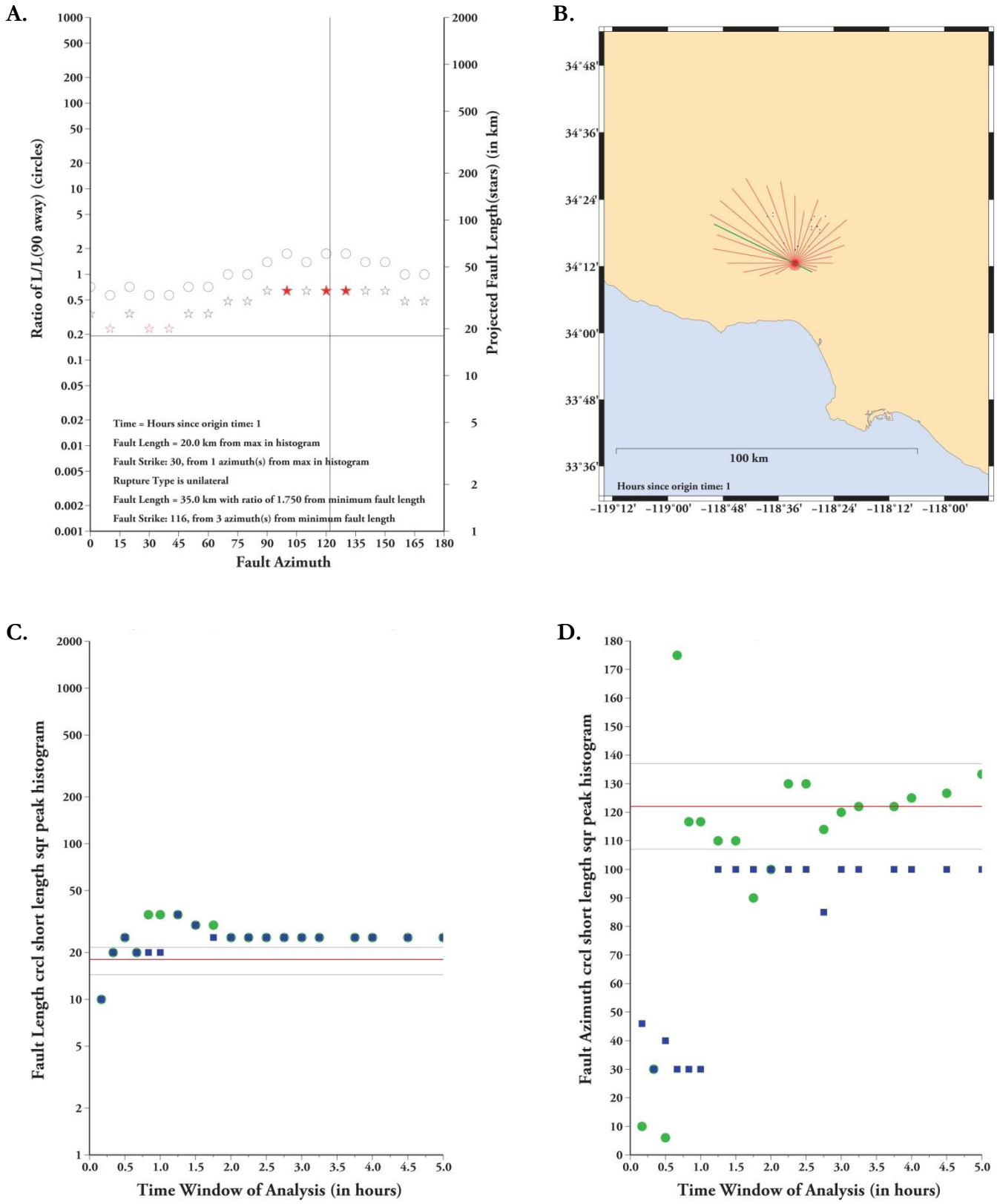

Figure 4: Results for the 1994 Mw 5.9 Double Springs, Nevada earthquake
(Captions for figures similar to Figure 2)

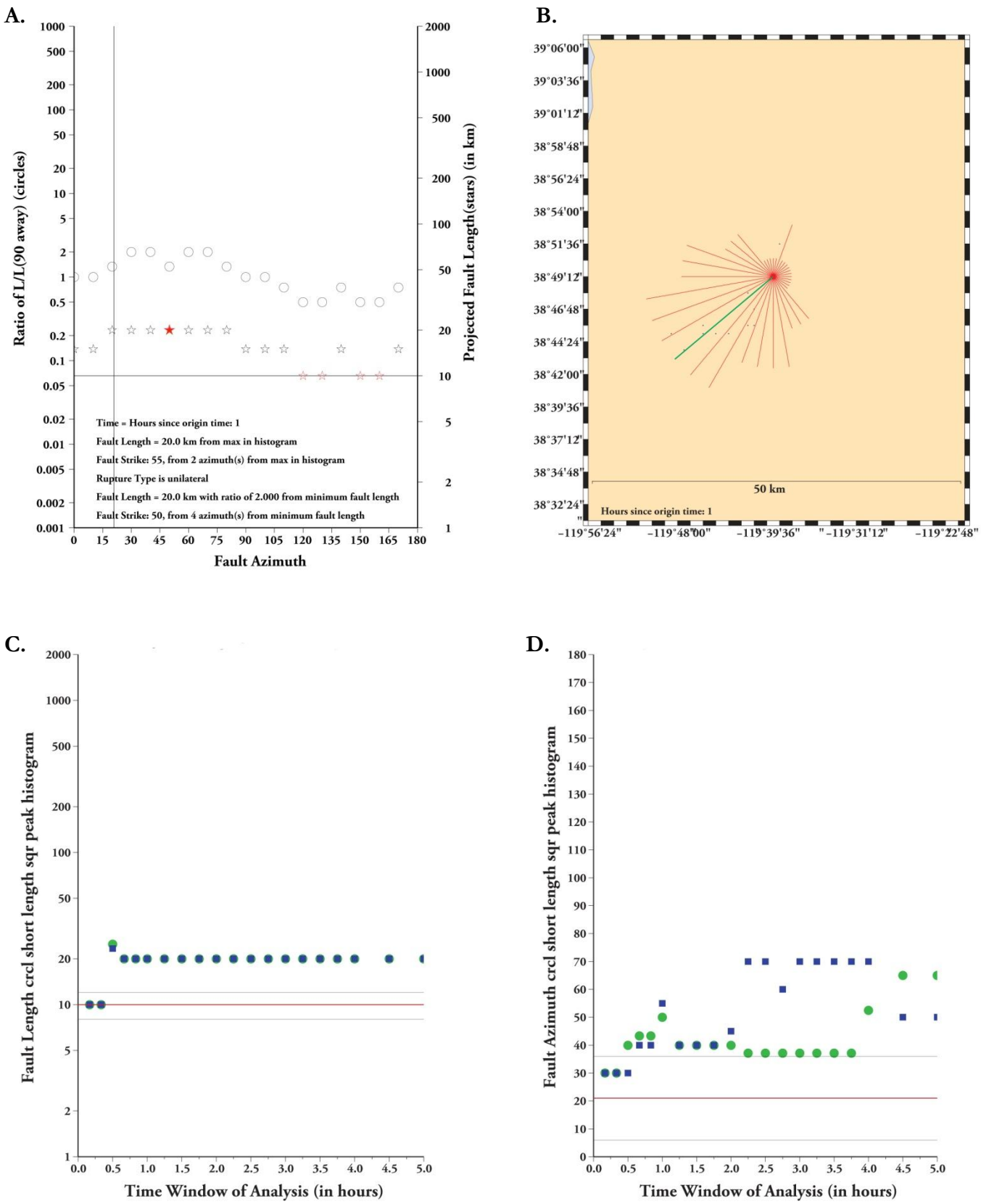

Results of fault length and strike using the minimum length and largest bin method are compared. We also determined the minimum amount of time within 5 hours that the algorithm produced the best constraining results for each earthquake to be compared to (see Tables 2 and 3). Further comparing our results, we plotted our calculated results against the results from the NGA database. Also, a "perfect answers" trend line was plotted to show how our calculated results came close to the NGA results (see Figures 5 and 6).

Table 2: Calculated results using largest bin method compared to NGA results

Event ID	Minutes since origin time	Calculated Fault Length (km)	NGA Fault Length (km)	Calculated Fault Strike (°azimuth)	NGA Fault Strike (°azimuth)
DI	135	10	12.6	100	130
CM	90	30	20	136	170
MA	50	60	71.6	30	112
CC	105	65	88	160	5
NO	60	20	18	30	122
HE	40	65	69	0	151
KJ	50	41.7	60	96	50
GR	210	25	17.5	40	54
DS	10	10	10	30	21
DU	20	50	46.8	90	85
ER	90	20	29	155	122
KG	20	28.1	27	85	55
KO	150	157.5	137.5	100	92
NM	40	25	30	70	83

Table 3: Calculated results using minimum length method compared to NGA results

Event ID	Minutes since origin time	Calculated Fault Length (km)	NGA Fault Length (km)	Calculated Fault Strike (°azimuth)	NGA Fault Strike (°azimuth)
DI	135	10	12.6	136	130
CM	90	35	20	150	170
MA	50	95	71.6	150	112
CC	105	70	88	170	5
NO	60	35	18	116	122
HE	40	65	69	175	151
KJ	50	55	60	130	50
GR	210	40	17.5	40	54
DS	10	10	10	30	21
DU	20	50	46.8	95	85
ER	90	20	29	155	122
KG	20	50	27	55	55
KO	150	165	137.5	90	92
NM	40	25	30	70	83

Figure 5: Largest bin method results vs. NGA results

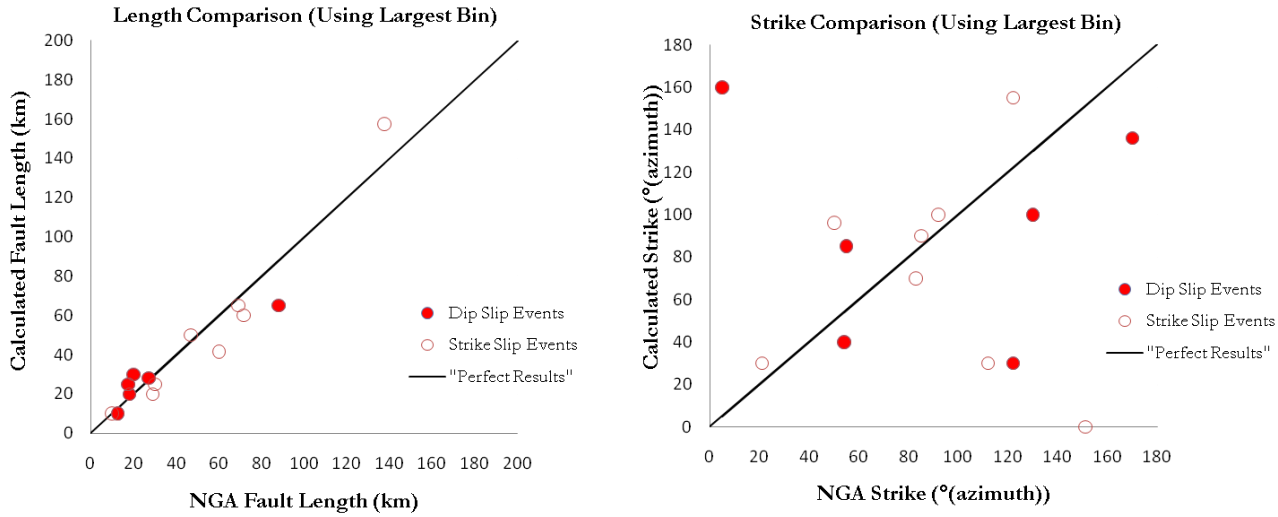

Figure 6: Minimum length method results vs. NGA results

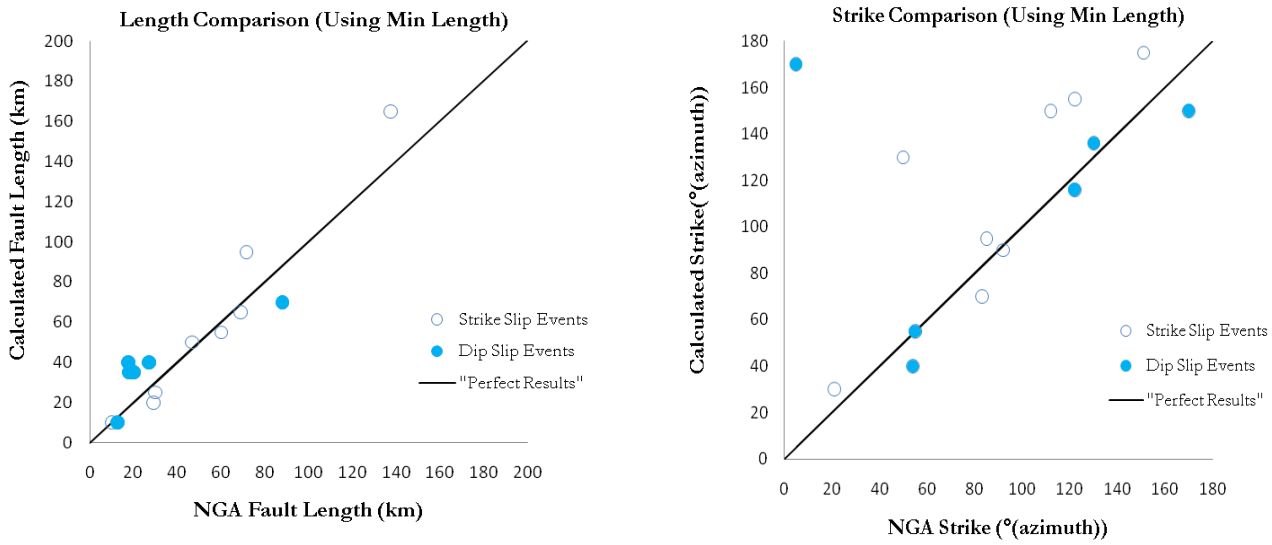

We see that fault rupture lengths compared better to with the NGA results than results for fault strikes. But we also observe that in terms of determining more constrained fault strikes, the minimum length method (picking the fault length 90° from the shortest aftershock distribution length) is again the better method. Aside from testing earthquakes in the NGA database we tested recent earthquakes and compared results to rupture models from full inversions as well. We believe comparing rupture parameters determined from full inversions of recent earthquakes provides more reliable results.

Recent Earthquakes Resulting in Large Fatalities

Over the past ten years there have been a number of large earthquakes that have resulted in fatalities of more than 1,000. This set of destructive earthquakes gives an incentive to look at their initial aftershock distribution and test them in our algorithm.

Unlike the NGA results, we do not have a singular objective source to compare this new set of earthquakes to. Rather, we are comparing these recent events to parameters determined from various earthquake source inversions. Earthquake rupture models derived from finite source inversions are nowadays the most routinely and modern approach for imaging the earthquake rupture process. However there are varieties of inversion and modeling approaches for earthquake rupture using different processing and data sets. Different sets of seismic data with supplementary geologic information and also approaches using geodetic data can produce different types of rupture models. As a result, different research teams using different inversion approaches can produce their own source model that may not agree with other models for the same given earthquake.

We researched different inversion models for our recent set of earthquakes and found a range of different rupture parameters for each earthquake. Finding constrained parameters for rupture length was more of a challenge than finding constrained parameters for fault strike. We found a minimum to a maximum range of rupture length parameters from rupture models available in literature and online and used that range to compare to our calculated rupture length parameters. Finding constrained fault strike parameters determined from full inversions however, was more straightforward and therefore we compared our results to a singular constrained strike parameter for each earthquake

We compared our calculated results using both the largest bin method and the minimum length method to the parameters determined from full inversions and our results show again that the minimum length method produced fault strikes that more closely agreed with those from the rupture models (See Appendix B). Therefore we will now show analysis of results only from the minimum length method.

Overall, our results for this set of recent destructive earthquakes produced more reliable results in our algorithm than the selected events from the NGA database. We show examples of our results with illustrations and figures similarly explained for the NGA "figures" however only showcasing results from the minimum length method with our results compared to results from full inversions.

Mw ≥ 9 Megathrust Earthquake Ruptures

There are two magnitude ≥ 9 events in our recent set of earthquakes that we studied: the 2011 Tohoku, Japan and 2004 Indian Ocean earthquake. Both earthquakes are large reverse subduction zone events that generated a massive tsunami. The mainshock size and rupture of both events were surprising in different and similar ways. The magnitude 9.0 Tohoku earthquake was somewhat surprising because only a few Mw > 8.0 have been reported for the past 1200 years in that area. We also expected the rupture length for an earthquake of this magnitude to be at least 480 km. However rupture models from full inversions and best constrained results from our algorithm indicate a shorter rupture length of approximately 250 to 300 km (see Figure 7).

The magnitude 9.1 – 9.3 Indian Ocean (also known as the Sumatra Andaman Islands) earthquake was also an event that seemed unexpected. This is because the earthquake occurred in an area of the subduction zone that was seen as unlikely to produce a magnitude of ≥ 9. Waveform inversions and rupture models indicated a minimum rupture length of the mainshock to be approximately 1200 km north-northwest along the Andaman trough. We see comparable results from our algorithm using initial aftershock locations determining a rupture length of 1080 km at 90 minutes from the origin time of the mainshock (see Figure 8).

Non Elongated Rupture Planes

We looked at mainshock ruptures that we consider being less rectangular and elongated and compare how constrained they are to our calculated results. The 2009 magnitude 7.6 Southern Sumatra earthquake rupture area was not very elongated and it is unclear which of the nodal planes of the mechanism corresponds to the fault plane. The finite fault model from full inversions provided at the USGS website shows 2 fault plane solutions with the mainshock plane being unsolved (Gavin Hayes, 2009). Plane 1 from the fault plane solution suggests a strike of 71.3º and plane 2 suggest a strike of 189.5º. Our best calculated results for the Southern Sumatra event is 90º (see Figure 9). We found that the aftershock distribution for this event was rather square-shaped and as a result our results for this event was not well constrained. The rupture area of the 2001 magnitude 7.7 Gujarat, India earthquake was also considered to be relatively less elongated but we obtained reliable rupture parameters that matched with parameters from full inversions within 90 minutes after the mainshock event (see Figure 10). After 90 minutes our algorithm determined less reliable rupture parameters.

Well Constrained Events

The 2008 magnitude 7.9 Eastern Sichuan, China earthquake is an example of an event that we obtained well matched rupture parameters compared to full inversions. The unilateral north-east rupture of the mainshock resulted in a long narrow distribution of aftershocks. We were able to obtained reliable rupture parameters of this event from early aftershock locations of 30 minutes after the mainshock. After 30 minutes, our algorithm continued to provide reliable rupture parameters hours after the mainshock. The Sichuan earthquake overall is an example of an event that illustrates how our approach of reliably determining rupture parameters works best for large mainshock ruptures with early aftershock distributions delineating a roughly narrow rectangular plane.

The 2010 magnitude 7.0 Port-au-Prince, Haiti earthquake is another example of an event that we obtained well matched rupture parameters but not as well as the Sichuan earthquake. We obtained results of fault strikes that seem consistent to a finite rupture model (Hayes, 2010) indicating an 84º azimuth fault plane suggesting a strike slip faulting mechanism on the Enriquillo-Plantain Garden fault system. However an updated study using GPS and radar interferometry measurements infers that the recent Haiti earthquake did not occur on the Enriquillo–Plantain Garden fault but rather on a previously unmapped north-dipping blind thrust fault that is newly named the Léogâne fault with the source mechanism being a combination of left-lateral strike-slip and reverse slip (Calais et al, 2010). The rupture estimates of the new study and previous rupture models are consistent with our determined fault length in the range of 30 to 35 km (though with later results after 180 minutes our rupture lengths were overestimated).

Figure 7: Results for the 2011 Mw 9.0 Tohoku, Japan earthquake

(Captions for figures similar to Figure 2 but with results only from min length method)

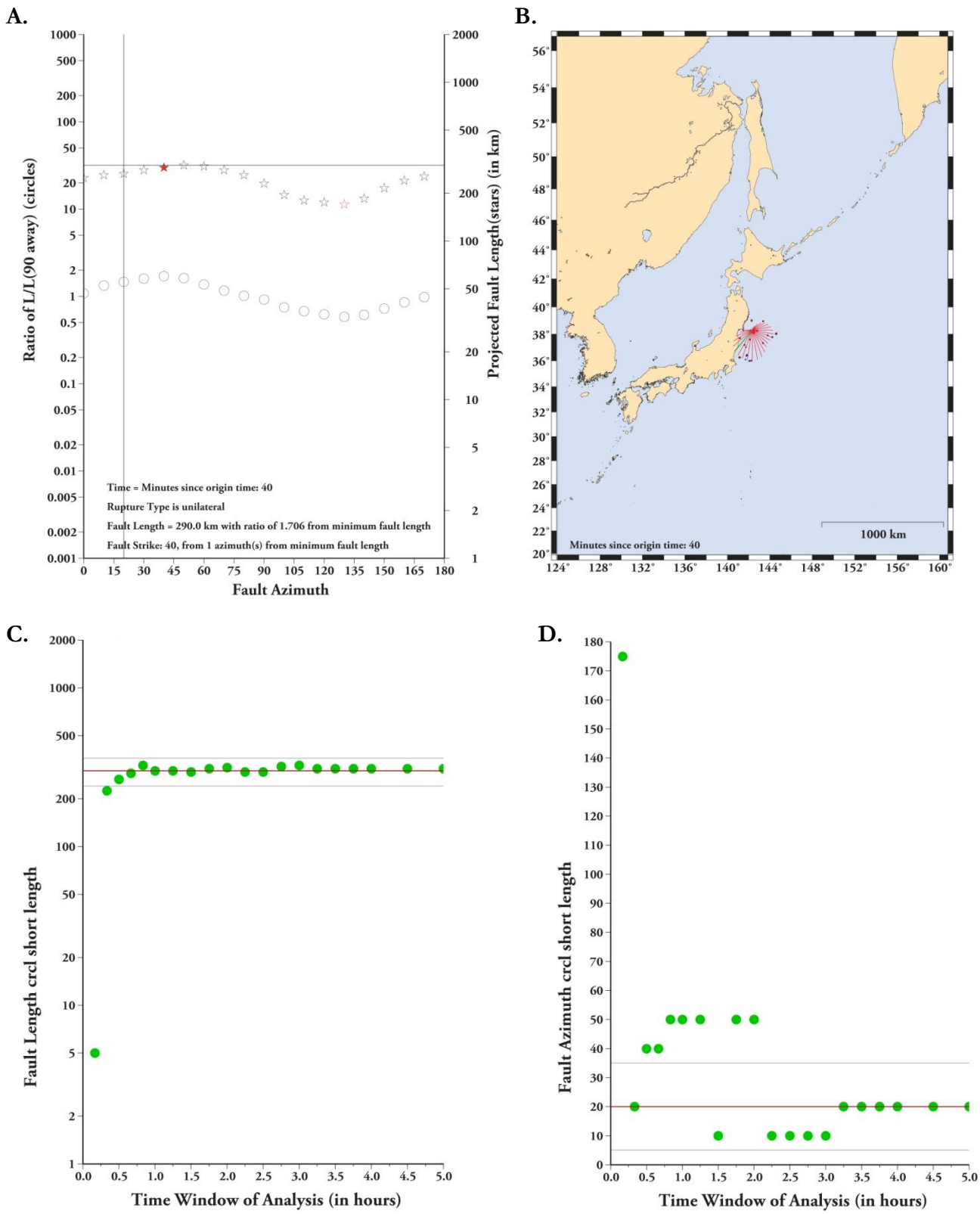

Figure 8: Results for the 2004 Mw 9.1 Indian Ocean earthquake

(Captions for figures similar to Figure 2 but with results only from min length method)

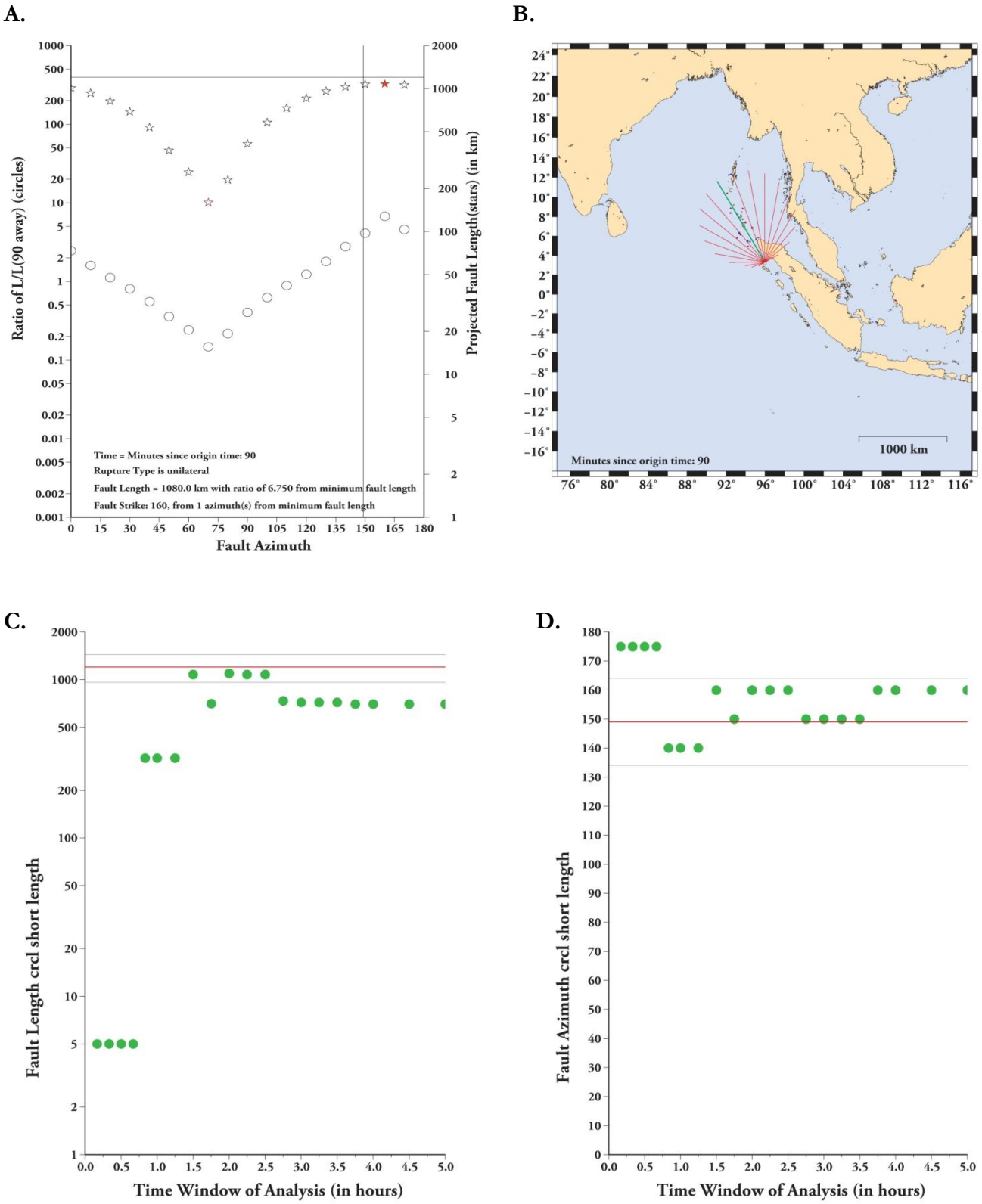

Figure 9: Results for the 2009 Mw 7.6 Southern Sumatra earthquake

(Captions for figures similar to Figure 2 but with results only from min length method)

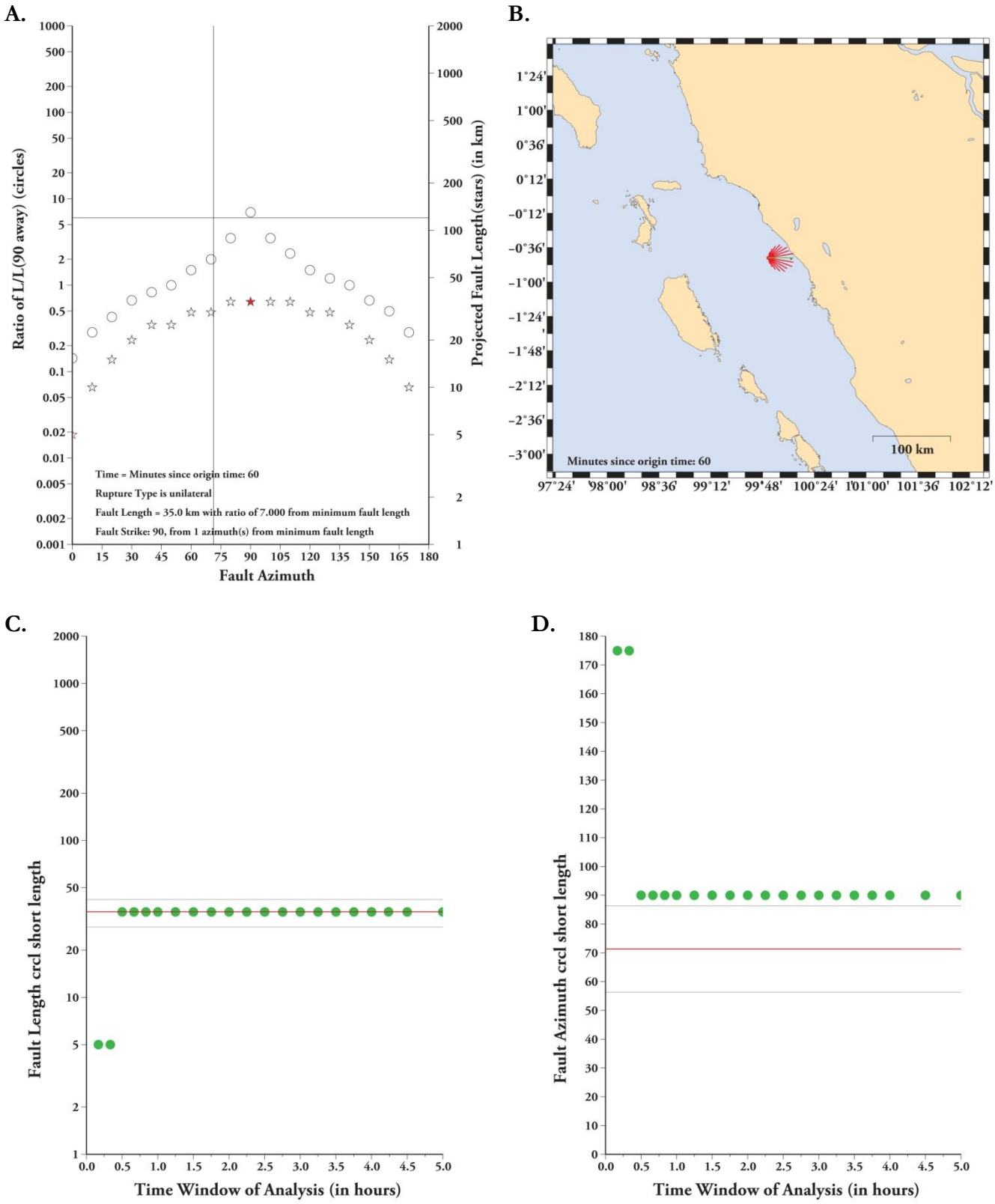

Figure 10: Results for the 2001 Mw. 7.7 Gujarat, India earthquake

(Captions for figures similar to Figure 2 but with results only from min length method)

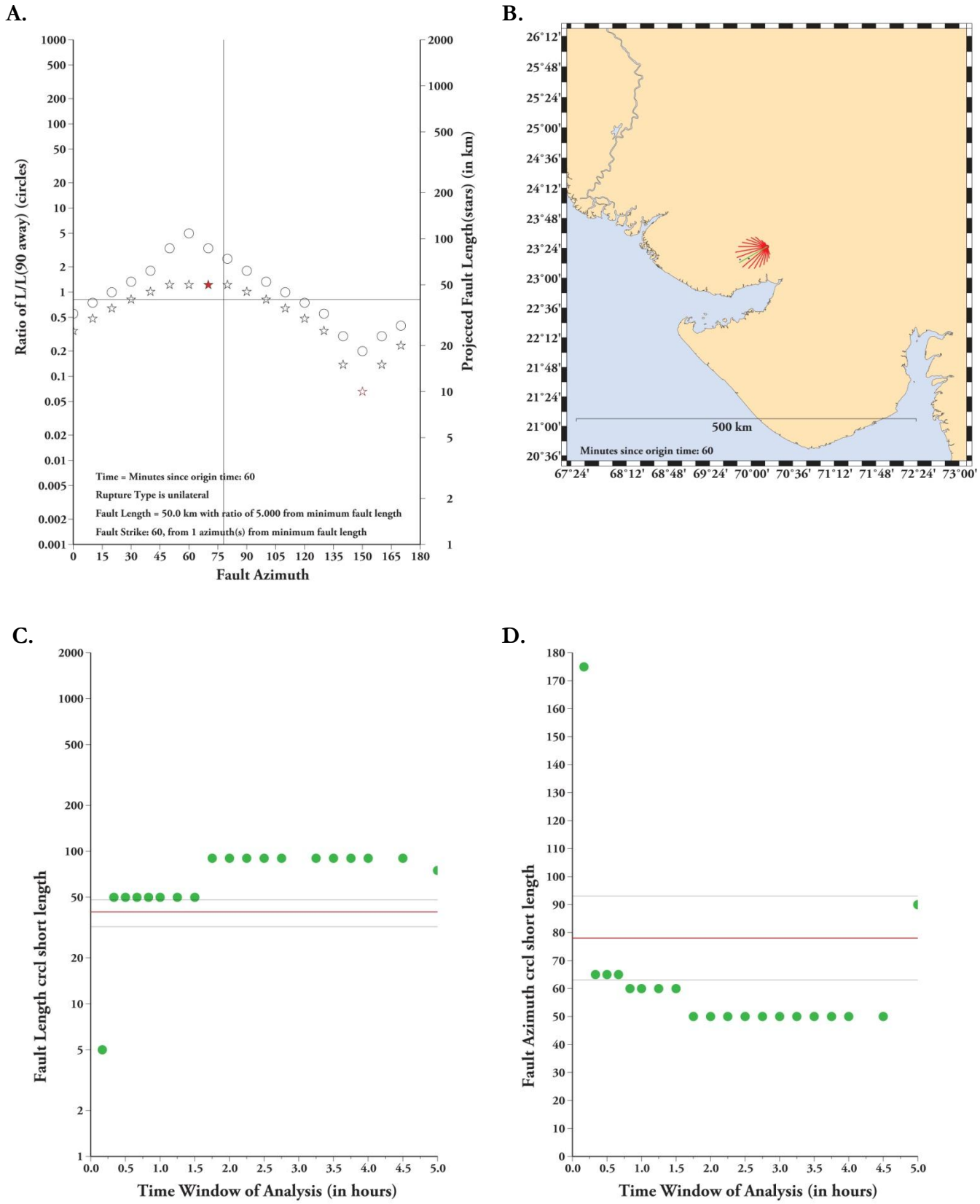

Figure 11: Results for the 2008 Mw 7.9 Eastern Sichuan, China Earthquake

(Captions for figures similar to Figure 2 but with results only from min length method)

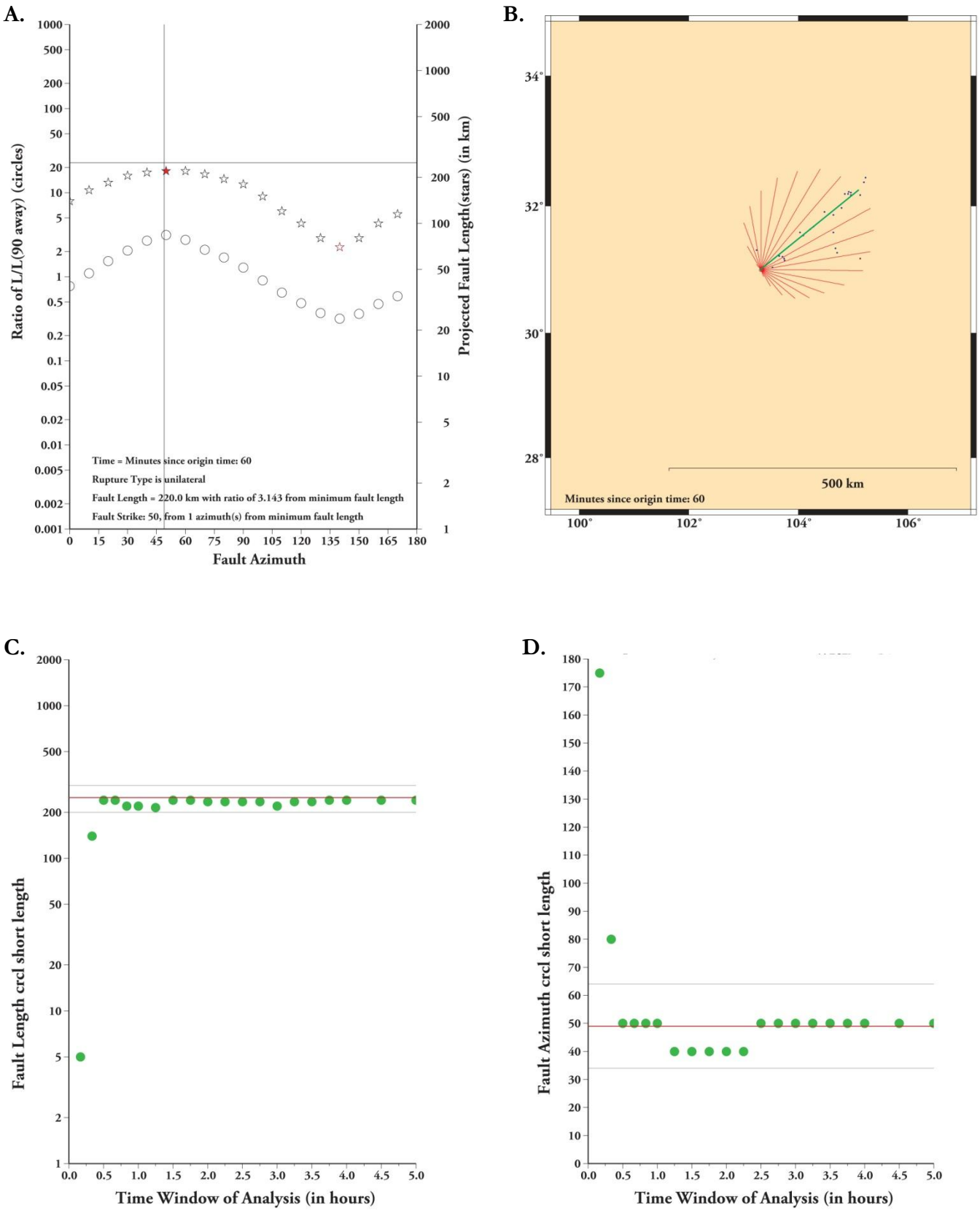

Figure 12: Results for the 2010 Mw 7.0 Haiti earthquake

(Captions for figures similar to Figure 2 but with results only from min length method)

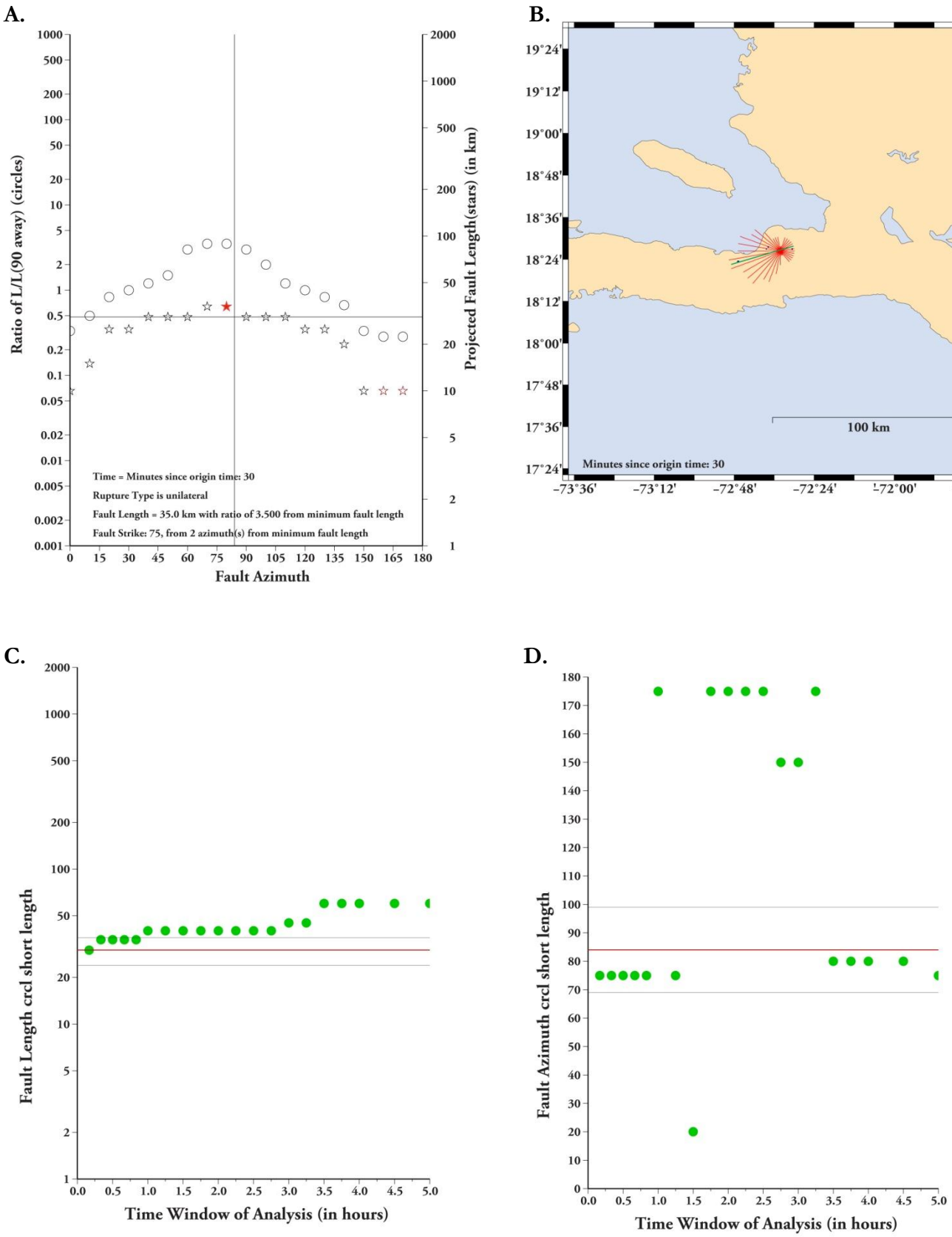

Accessing the Effectiveness of Our Algorithm

We want to investigate how well our algorithm can determine reliable rupture parameters as a function of time to receive a better understanding of when the method works well. We used our list of recent destructive earthquakes as our events to test how reliable our algorithm is. There are a total of 10 events from this list and we computed the percentage of how many events of the total 10 events determined reliable rupture parameters for rupture length and strike as a function of time (up to 5 hours or 300 minutes). The criteria as to whether a result was well determined were based on whether it matched to rupture models from full inversions (rupture lengths were compared to a range of values). The uncertainty values we gave were ±20% (Figure 13A), ±30% (Figure 13C) for rupture length, ±20° (Figure 13B), ±30° (Figure 13D) for strike.

Figure 13: Percentages of successfully determined rupture parameters vs. time

A.

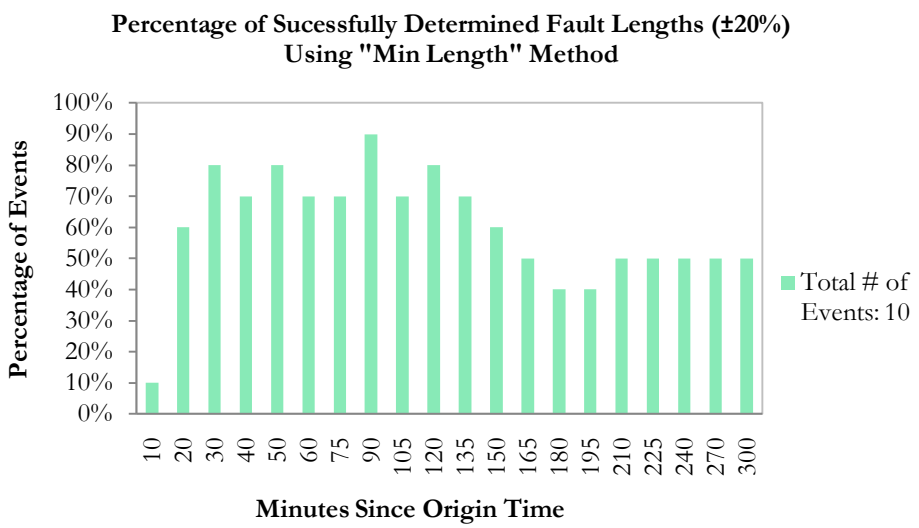

B.

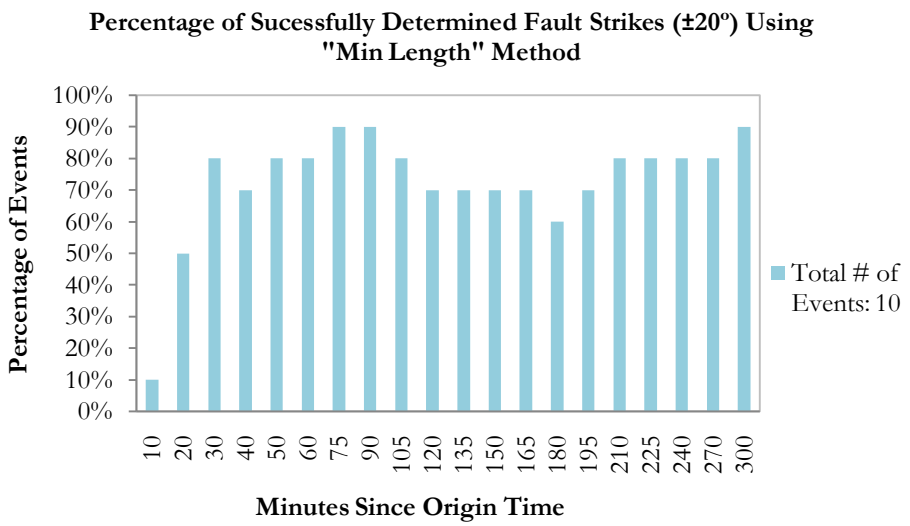
Percentage of Sucessfully Determined Fault Strikes (±20º) Using "Min Length" Method
Percentage of Events
100%
90%
80%
70%
60%
50%
40%
30%
20%
10%
0%
10
20
30
40
50
60
75
90
105
120
135
150
165
180
195
210
225
240
270
300
Minutes Since Origin Time
Total # of Events: 10

C.

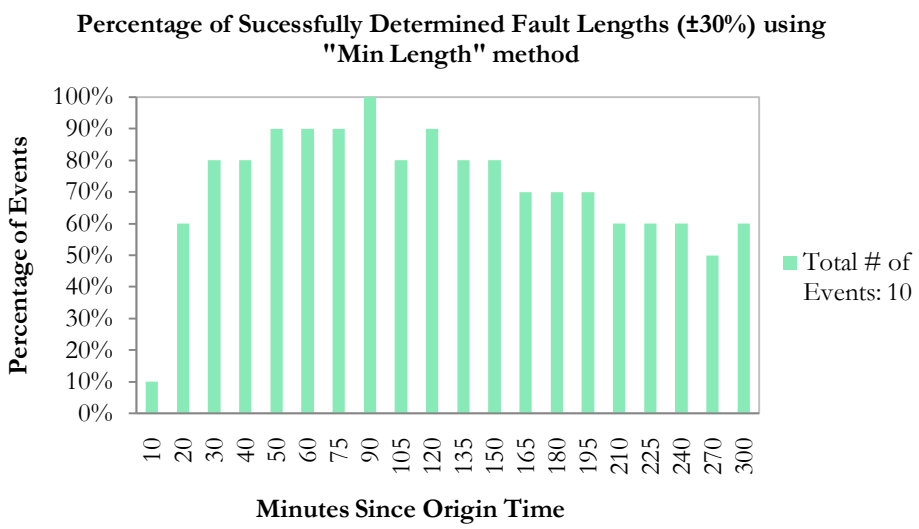
Percentage of Sucessfully Determined Fault Lengths (±30%) using "Min Length" method
Percentage of Events
100%
90%
80%
70%
60%
50%
40%
30%
20%
10%
0%
10
20
30
40
50
60
75
90
105
120
135
150
165
180
195
210
225
240
270
300
Minutes Since Origin Time
Total # of Events: 10

D.

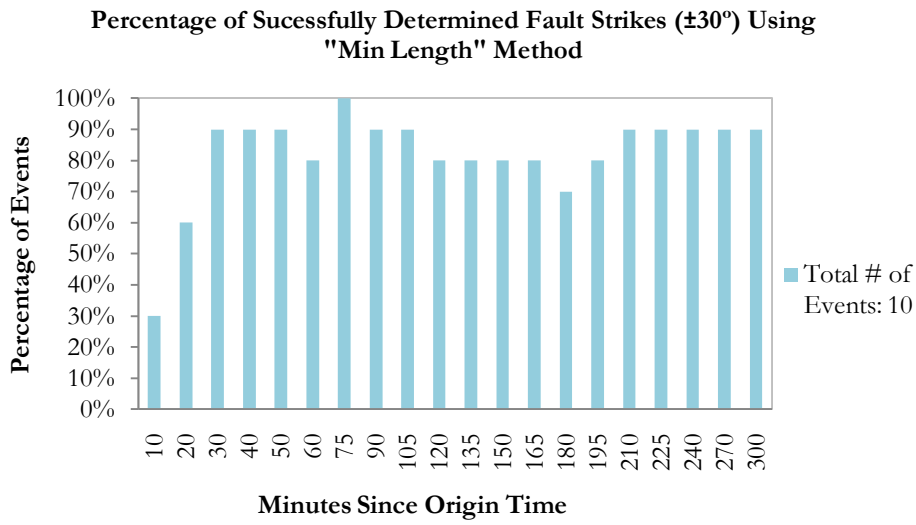

We also plotted the results of rupture length and strike within 60 minutes of the mainshock against results determined from full inversions with the ±20% rupture length and ±20° strike uncertainty value.

Figure 14: Calculated rupture parameters vs. rupture parameters from full inversions

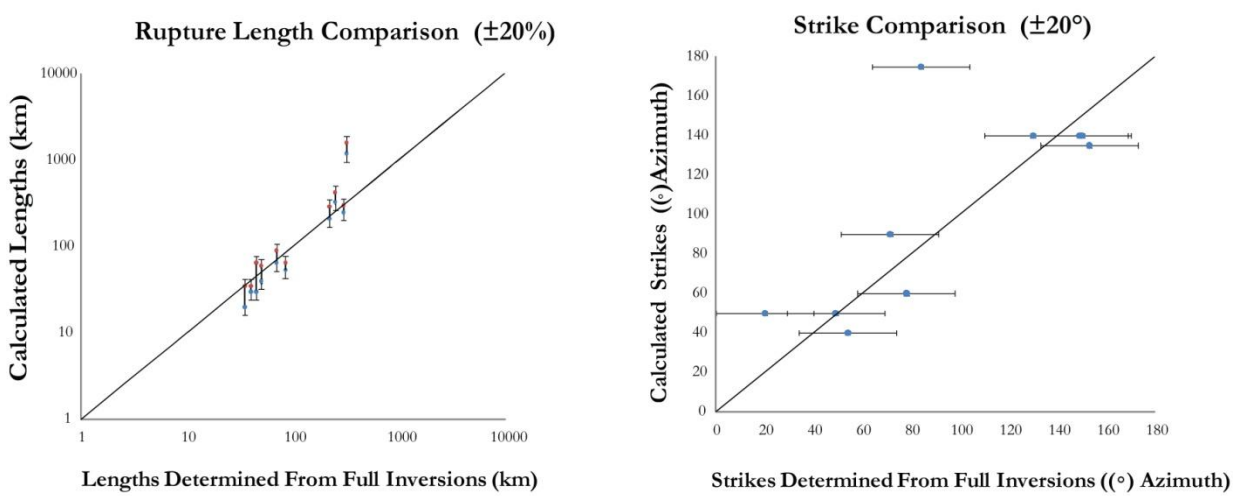

Our plots indicate that we can obtain reliable rupture parameters starting after 30 minutes of the mainshock for both determining rupture length and strike. However, our histograms indicate that after the first couple of hours we obtain less reliable rupture parameter results for determining rupture length. But we obtain more consistency with determining reliable strikes. Fault length results listed in Appendix B indicate that most events (such as the Haiti earthquake) resulted in longer fault lengths as a function of time. We can infer that obtaining rupture lengths using aftershocks is most useful during its very early distribution as the issue of obtaining less reliable rupture lengths may be due to aftershocks diffusing away from the mainshock rupture area as more time passes.

Discussing Algorithm Improvement

For the results of the 2011 Tohoku, Japan and the 2004 Indian Ocean earthquake, we observe that our algorithm incorrectly separated true aftershocks from triggered events. As a result, there were many true aftershock locations that were not used in the calculation by our algorithm. Although we were able to obtain constrained rupture parameters as indicated earlier from these events (although less so for the Indian Ocean quake), we believe the issue of our outlier removal and true aftershock criteria for our algorithm needs to be readdress. For large earthquakes such as a Magnitude 9 or greater that results in a large rupture area, aftershocks will commonly be distributed over a large distance from each other and as a result are not as constrained to the "closeness parameter" that is currently fixed in our algorithm to distinguish outlier events.

We can implement a different outlier removal parameter depending on the initial mainshock magnitude. If the outlier removal parameter is improved, a more reliable aftershock distribution can be computed in the algorithm. We can also suggest an additional step to manually remove outliers before running the algorithm and then compare results to the results from the fully automated algorithm to see how well the results are constrained.

Conclusions

We show that within 30 minutes after a large mainshock, reliable rupture parameters may be determined by our algorithm, indicating that this method based on early aftershock distributions works well. However, we find that not all of the events we tested were well constrained. Results for rupture lengths increased to values larger than the length determined by rupture inversions after a few hours had passed since the mainshock, but strike results were well matched over the entire time

period. This may be related to aftershocks diffusing and evolving away from the mainshock rupture area over time. The earthquakes that did not work as well with our algorithm had mainshock ruptures planes that are less rectangular and more squared shaped (such as the 2009 Southern Sumatra earthquake). In contrast, a long rectangular rupture area delineates the fault length much better (such as the 2008 Sichuan, China earthquake) and as such, our method works best for determining parameters for that type of mainshock rupture.

An automated algorithm that rapidly determines first-order mainshock rupture parameters such as ours can provide fast and useful input about faulting geometry and rupture direction. Knowing the initial distribution of aftershocks after a significant earthquake thus provides useful information that can help assess the scope of an earthquake disaster. We therefore conclude that locating early aftershock locations quickly is important for aiding earthquake response.

References

Ayadi, A., C. Dorbath, F. Ousadou, S. Maouche, M. Chikh, M. A. Bounif, and M. Meghraoui (2008), Zemmouri earthquake rupture zone (M_w 6.8, Algeria): Aftershocks sequence relocation and 3D velocity model, J. Geophys. Res., 113, B09301, doi:10.1029/2007JB005257.

Chen, Ji, and Gavin Hayes. "Finite Fault Model: Preliminary Result of the May 12, 2008 Mw 7.9 Eastern Sichuan, China Earthquake." U.S. Geological Survey Earthquake Hazards Program. USGS. Web. 27 January 2011. <http://earthquake.usgs.gov/earthquakes/eqinthenews/2008/us2008ryan/finite_fault.php>.

Chen Ji, Xiangyu Li, and Shao, Guangfu. "Preliminary Result for Rupture Process of Mar 11, 2011 Mw 9.11 Honshu Earthquake." UCSB Earth Science : Home. UCSB. Web. 27 January 2011. <http://www.geol.ucsb.edu/faculty/ji/big_earthquakes/2011/03/0311/Honshu.html>.

Das, S. and C. Henry, 2003. Spatial relation between main earthquake slip and its aftershock distribution, Rev. of Geophys., 41, 3, doi:10.1029/2002RG000119.

Earle, P.S., Wald, D.J., Jaiswal, J.S., Allen, T.I., Marano, K.D., Hotovec, A.J., Hearne, M.G., and Fee, J.M. (2009). Prompt Assessment of Global Earthquakes for Response (PAGER): A system for rapidly determining the impact of global earthquakes worldwide: U.S. Geological Survey Open File Report 2009-1131

Eric Calais, Andrew Freed, Glen Mattioli, Falk Amelung, Sigurjón Jónsson, Pamela Jansma, Sang-Hoon Hong, Timothy Dixon, Claude Prépetit, Roberte Momplaisir. Transpressional rupture of an unmapped fault during the 2010 Haiti earthquake. Nature Geoscience, 2010

Hao Zhang and Zengxi Ge. Tracking the Rupture of the 2008 Wenchuan Earthquake by Using the Relative Back-Projection Method. Bulletin of the Seismological Society of America, Nov 2010; 100: 2551 - 2560.

Hayes, Gavin. "Finite Fault Model: Preliminary Result of the Sep 30, 2009 Mw 7.6 Southern Sumatra Earthquake." U.S. Geological Survey Earthquake Hazards Program. USGS. Web. 27 January 2011. <http://earthquake.usgs.gov/earthquakes/eqinthenews/2009/us2009mebz/finite_fault.php>.

Hayes, Gavin. "Finite Fault Model: Updated Result of the Jan 12, 2010 Mw 7.0 Haiti Earthquake " U.S. Geological Survey Earthquake Hazards Program. Web. 27 January 2011. <http://earthquake.usgs.gov/earthquakes/eqinthenews/2010/us2010rja6/finite_fault.php>.

Hayes, Gavin. "Finite Fault Model: Updated Result of the Sep 3, 2010 Mw 7.0 Darfield, South Island New Zealand Earthquake." U.S. Geological Survey Earthquake Hazards Program. Web. 11 Nov. 2010. <http://earthquake.usgs.gov/earthquakes/eqinthenews/2010/us2010atbj/finite_fault.php>.

Henry, C. and S. Das, Aftershock zones of large shallow earthquakes: fault dimensions, aftershock area expansion and scaling relations, Geophys. J. Int, 147, 272-293.

Huang, B. S., Y. L. Huang, P. L. Leu and S. J. Lee (2011) Estimation of the rupture velocity and fault length of the 2004 Sumatra–Andaman earthquake using a dense broadband seismic array in Taiwan. J. Asian Earth Sciences, 40, 762-769, doi:10.1016/j.jseaes.2010.10.020. IESAS1537

Hutko, A.R. Lay, T. and Koper, K. D. Imaging the ruptures of the 2009 Samoan and Sumatran earthquakes using broadband network back-projections: Results and limitations. American Geophysical Union, Fall Meeting 2009, abstract #U22B-02

Ji, Chen. "Preliminary Result for Slip History of 05/10/08 PAKISTAN Earthquake." U.S. Geological Survey Earthquake Hazards Program. USGS. Web. 27 January 2011. <http://earthquake.usgs.gov/earthquakes/eqinthenews/2005/usdyae/finitefault/>.

José Fernando Borges, Bento Caldeira and Mourad Bezzeghoud. Source Rupture Process of the Sumatra, Indonesia Earthquake (Mw=8.6) of 28 March 2005Preliminary Results. < http://www.emsc-csem.org/Doc/SUMATRA_280305/Sumatra-rupture-process-M282005.pdf >

Lay, T., et. al., The Great Sumatra-Andaman earthquake of 26 December 2004, Science, 308, 1127-1133, 2005. Supported by NSF grants EAR-0125595, EAR-0337495, EAR-0207608, and Cooperative Agreement EAR-0004370

Mandal, P., Horton, S., (2006), Relocation of aftershocks, focal mechanisms and stress inversion: Implications toward the seismo-tectonics of the causative fault zone of Mw7.6 2001 Bhuj earthquake (India), 2006,Science Direct, Tectonophysics 429 (2007) 61–78

Meghraoui, M., et al. (2004), Coastal uplift and thrust faulting associated with the M_w = 6.8 Zemmouri (Algeria) earthquake of 21 May, 2003, Geophys. Res. Lett., 31, L19605, doi:10.1029/2004GL020466.

Negishi, H., J. Mori, T. Sato, R. Singh, S. Kumar, and N. Hirata (2002), Size and orientation of the fault plane for the 2001 Gujarat, India earthquake (Mw7.7) from aftershock observations: A high stress drop event, Geophys. Res. Lett., 29(20), 1949, doi:10.1029/2002GL015280.

PEER NGA Database: Browse Earthquakes. Welcome to Pacific Earthquake Engineering Research Center - PEER. Web. 19 August 2010. <http://peer.berkeley.edu/nga/earthquakes.html>.

Shao, Guangfu, and Chen Ji. "Preliminary Result for Rupture Process of Mar 28, 2005 Mw 8.68 Nais Earthquake." UCSB Earth Science. Web. 27 January 2011. <http://www.geol.ucsb.edu/faculty/ji/big_earthquakes/2005/03/smooth/nias.html>.

Semmane, F., Campillo, M. and Cotton, F., 2005. Fault location and source process of the Boumerdes, Alge_ria, earthquake inferred from geodetic and strong motion data. Geophys. Res. Lett., 32(1): L01305.

Sladen, Anthony. "Slip-History Database :: 2009 Padang Earthquake." Tectonics Observatory at Caltech. Caltech. Web. 27 January 2011. <http://www.tectonics.caltech.edu/slip_history/2009_padang/padang.html>.

Wei, Shengji, Anthony Sladen, and ARIA Group. "Slip-History Database :: 2011 Tohoku-oki Earthquake." Tectonics Observatory at Caltech. Web. 5 May 2011. <http://www.tectonics.caltech.edu/slip_history/2011_taiheiyo-oki/>.

Yuichiro Tanioka, Yudhicara, Tomohiro Kususose, S. Kathiroli, Yuichi Nishimura, Sin-Iti Iwasaki, and Kenji Satake. Rupture process of the 2004 great Sumatra-Andaman earthquake estimated from tsunami waveforms. Earth Planets Space, Vol. 58 (No. 2), pp. 203-209, 2006

Zhang, H., and Z. Ge (2010). Tracking the rupture of the 2008 Wenchuan earthquake by using the relative back-projection method, Bull. Seismol. Soc. Am. 100, no. 5B, 2551–2560.
Zhang Y, Xu L S, Chen Y T. Source process of the 2010 Yushu, Qinghai, earthquake. Sci China Earth Sci, 2010, 53: 1249–1251, doi: 10.1007/s11430-010-4045-5

Appendix A

Detailed Results for the 2010 Canterbury, New Zealand Earthquake

On September 03, 2010 a magnitude 7.0 earthquake struck the South Island of New Zealand in the region of Canterbury and city of Christchurch at 16:35:46 UTC. New Zealand is located on the plate boundary between the Pacific and Australian plate, where the nature of the plate boundary changes from a subduction zone to a transform boundary cutting through the continental crust of the South Island as the Alpine Fault. The recent New Zealand earthquake started on a previously undetected fault line under the Canterbury Plains, a blind thrust fault that nearly instantaneously triggered the strike-slip Greendale fault, along which most of the slip took place. In the first few hours after the mainshock, it was unclear what type of faulting had occurred and which specific fault was responsible for the earthquake, due to the complicated tectonics of the region. The most common assumption was that the event must have occurred on an NE trending right lateral strike-slip fault, such as the Alpine fault.

By applying our methodology of using early aftershocks locations of the mainshock, we determined reliable fault rupture strike and length as early as 30 minutes to 90 minutes of the mainshock occurrence. From the aftershock distribution following the Canterbury quake, we used two aftershock catalogs to calculate the fault length and orientation: the National Earthquake Information Catalog (NEIC) and the local GeoNet (collaboration between the Earthquake Commission and GNS Science) catalog. Results were constrained to the minimum time to fit the strike and fault length values of 85º and 50 km, as determined in the days following the mainshock by detailed seismic waveform modeling performed by the USGS. By using the NEIC catalog for .5 hr (30 min), calculated results indicated a fault length of 55 km and 80º by using the minimum length method. Using the GeoNet catalog for up to 1.5 hrs (90 min) resulted in a fault length of 45 km and 75º strike by using the minimum length method.

Figure 15: Detailed results for the 2010 Mw 7.0 Canterbury, New Zealand earthquake

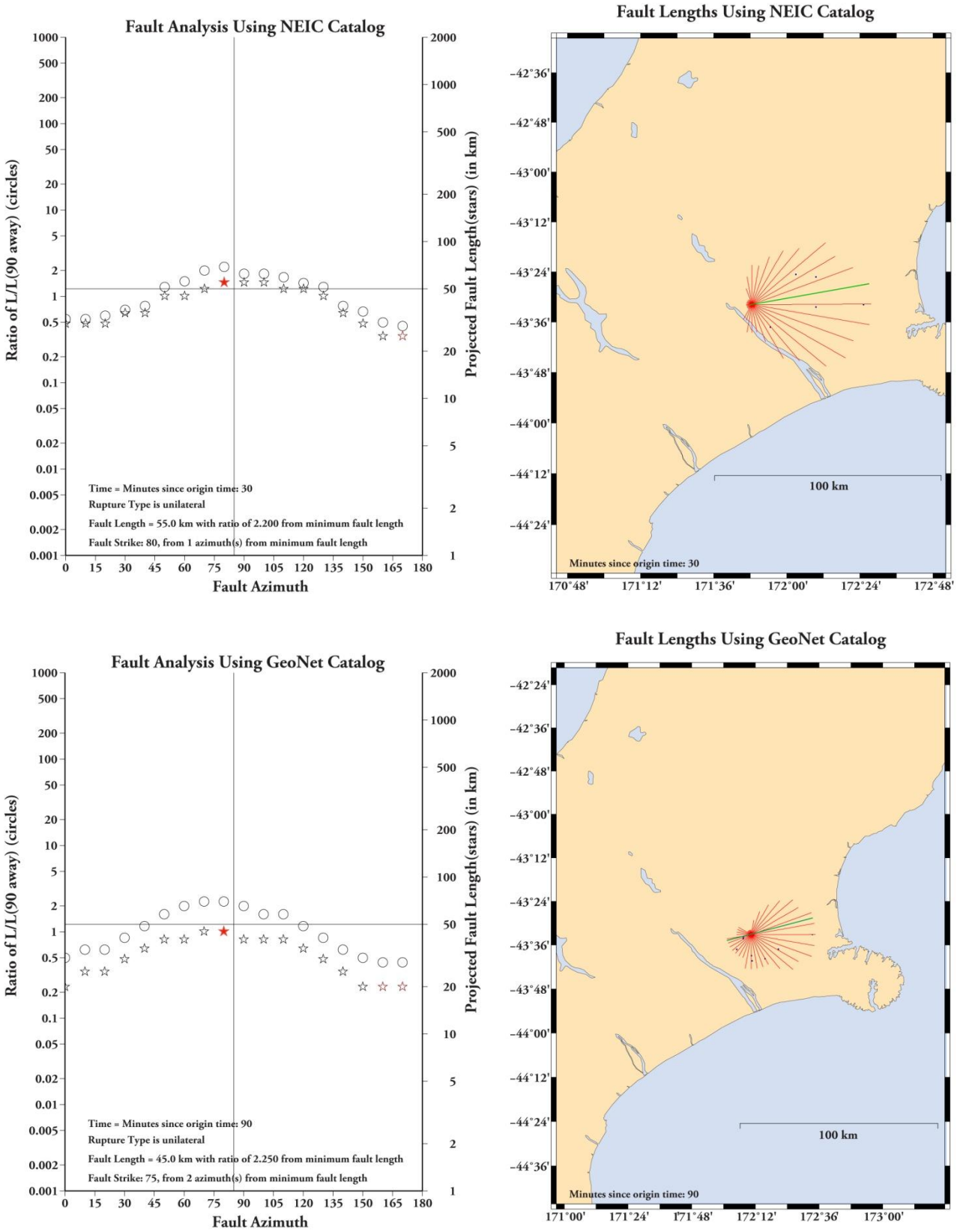

Appendix B

Rupture Parameters of Recent Destructive Earthquakes

Table 4: Calculated rupture parameters and reliable rupture parameters (from full inversions)

Event ID	Minutes since origin time	Calculated Fault Length (km)	Calculated Fault Strike °Azimuth	Reliable Fault Length Range (km)	Reliable Fault Strike °Azimuth	±20% (Length)	±30% (Length)	±20° (Strike)	±30° (Strike)
YU	10	5	85	(30-65)	130	✗	✗	✗	✗
YU	10	5	175	(30-65)	130	✗	✗	✗	✗
YU	20	24.2	66	(30-65)	130	✓	✓	✗	✗
YU	20	45	140	(30-65)	130	✓	✓	✓	✓
YU	30	31.1	76	(30-65)	130	✓	✓	✗	✗
YU	30	45	140	(30-65)	130	✓	✓	✓	✓
YU	40	31.1	76	(30-65)	130	✓	✓	✗	✗
YU	40	45	140	(30-65)	130	✓	✓	✓	✓
YU	50	31.1	76	(30-65)	130	✓	✓	✗	✗
YU	50	45	140	(30-65)	130	✓	✓	✓	✓
YU	60	31.1	76	(30-65)	130	✓	✓	✗	✗
YU	60	45	140	(30-65)	130	✓	✓	✓	✓
YU	75	45	20	(30-65)	130	✓	✓	✗	✗
YU	75	65	130	(30-65)	130	✓	✓	✓	✓
YU	90	45	20	(30-65)	130	✓	✓	✗	✗
YU	90	65	130	(30-65)	130	✓	✓	✓	✓
YU	105	57.5	75	(30-65)	130	✓	✓	✗	✗
YU	105	70	130	(30-65)	130	✓	✓	✓	✓
YU	120	61.7	93	(30-65)	130	✓	✓	✗	✗
YU	120	70	130	(30-65)	130	✓	✓	✓	✓
YU	135	61.7	93	(30-65)	130	✓	✓	✗	✗
YU	135	70	130	(30-65)	130	✓	✓	✓	✓
YU	150	61.7	93	(30-65)	130	✓	✓	✗	✗
YU	150	70	130	(30-65)	130	✓	✓	✓	✓
YU	165	61.7	93	(30-65)	130	✓	✓	✗	✗
YU	165	70	130	(30-65)	130	✓	✓	✓	✓
YU	180	61.7	93	(30-65)	130	✓	✓	✗	✗
YU	180	70	130	(30-65)	130	✓	✓	✓	✓
YU	195	61.7	93	(30-65)	130	✓	✓	✗	✗
YU	195	70	130	(30-65)	130	✓	✓	✓	✓
YU	210	70	130	(30-65)	130	✓	✓	✓	✓
YU	210	70	130	(30-65)	130	✓	✓	✓	✓
YU	225	70	130	(30-65)	130	✓	✓	✓	✓
YU	225	70	130	(30-65)	130	✓	✓	✓	✓
YU	240	70	130	(30-65)	130	✓	✓	✓	✓
YU	240	70	130	(30-65)	130	✓	✓	✓	✓
YU	270	70	130	(30-65)	130	✓	✓	✓	✓
YU	270	70	130	(30-65)	130	✓	✓	✓	✓
YU	300	70	130	(30-65)	130	✓	✓	✓	✓

YU	300	70	130	(30-65)	130	✓	✓	✓	✓
HA	10	30	75	(30-35)	84	✓	✓	✓	✓
HA	10	30	75	(30-35)	84	✓	✓	✓	✓
HA	20	31.7	90	(30-35)	84	✓	✓	✓	✓
HA	20	35	75	(30-35)	84	✓	✓	✓	✓
HA	30	31.7	90	(30-35)	84	✓	✓	✓	✓
HA	30	35	75	(30-35)	84	✓	✓	✓	✓
HA	40	31.7	90	(30-35)	84	✓	✓	✓	✓
HA	40	35	75	(30-35)	84	✓	✓	✓	✓
HA	50	31.7	90	(30-35)	84	✓	✓	✓	✓
HA	50	35	75	(30-35)	84	✓	✓	✓	✓
HA	60	40	90	(30-35)	84	✓	✓	✓	✓
HA	60	40	175	(30-35)	84	✓	✓	✗	✗
HA	75	40	90	(30-35)	84	✓	✓	✓	✓
HA	75	40	75	(30-35)	84	✓	✓	✓	✓
HA	90	40	90	(30-35)	84	✓	✓	✓	✓
HA	90	40	20	(30-35)	84	✓	✓	✗	✗
HA	105	40	85	(30-35)	84	✓	✓	✓	✓
HA	105	40	175	(30-35)	84	✓	✓	✗	✗
HA	120	40	90	(30-35)	84	✓	✓	✓	✓
HA	120	40	175	(30-35)	84	✓	✓	✗	✗
HA	135	40	90	(30-35)	84	✓	✓	✓	✓
HA	135	40	175	(30-35)	84	✓	✓	✗	✗
HA	150	40	90	(30-35)	84	✓	✓	✓	✓
HA	150	40	175	(30-35)	84	✓	✓	✗	✗
HA	165	40	90	(30-35)	84	✓	✓	✓	✓
HA	165	40	150	(30-35)	84	✓	✓	✗	✗
HA	180	45	85	(30-35)	84	✗	✓	✓	✓
HA	180	45	150	(30-35)	84	✗	✓	✗	✗
HA	195	45	90	(30-35)	84	✗	✓	✓	✓
HA	195	45	175	(30-35)	84	✗	✓	✗	✗
HA	210	55	90	(30-35)	84	✗	✗	✓	✓
HA	210	60	80	(30-35)	84	✗	✗	✓	✓
HA	225	55	90	(30-35)	84	✗	✗	✓	✓
HA	225	60	80	(30-35)	84	✗	✗	✓	✓
HA	240	55	90	(30-35)	84	✗	✗	✓	✓
HA	240	60	80	(30-35)	84	✗	✗	✓	✓
HA	270	55	90	(30-35)	84	✗	✗	✓	✓
HA	270	60	80	(30-35)	84	✗	✗	✓	✓
HA	300	55	90	(30-35)	84	✗	✗	✓	✓
HA	300	60	75	(30-35)	84	✗	✗	✓	✓
SS	10	5	85	(20-35)	71.3	✗	✗	✓	✓
SS	10	5	175	(20-35)	71.3	✗	✗	✗	✗
SS	20	5	85	(20-35)	71.3	✗	✗	✓	✓
SS	20	5	175	(20-35)	71.3	✗	✗	✗	✗
SS	30	35	90	(20-35)	71.3	✓	✓	✓	✓
SS	30	35	90	(20-35)	71.3	✓	✓	✓	✓
SS	40	35	90	(20-35)	71.3	✓	✓	✓	✓
SS	40	35	90	(20-35)	71.3	✓	✓	✓	✓
SS	50	35	90	(20-35)	71.3	✓	✓	✓	✓

SS	50	35	90	(20-35)	71.3	✓	✓	✓	✓
SS	60	35	90	(20-35)	71.3	✓	✓	✓	✓
SS	60	35	90	(20-35)	71.3	✓	✓	✓	✓
SS	75	35	90	(20-35)	71.3	✓	✓	✓	✓
SS	75	35	90	(20-35)	71.3	✓	✓	✓	✓
SS	90	35	90	(20-35)	71.3	✓	✓	✓	✓
SS	90	35	90	(20-35)	71.3	✓	✓	✓	✓
SS	105	35	90	(20-35)	71.3	✓	✓	✓	✓
SS	105	35	90	(20-35)	71.3	✓	✓	✓	✓
SS	120	35	90	(20-35)	71.3	✓	✓	✓	✓
SS	120	35	90	(20-35)	71.3	✓	✓	✓	✓
SS	135	35	90	(20-35)	71.3	✓	✓	✓	✓
SS	135	35	90	(20-35)	71.3	✓	✓	✓	✓
SS	150	35	90	(20-35)	71.3	✓	✓	✓	✓
SS	150	35	90	(20-35)	71.3	✓	✓	✓	✓
SS	165	35	90	(20-35)	71.3	✓	✓	✓	✓
SS	165	35	90	(20-35)	71.3	✓	✓	✓	✓
SS	180	35	90	(20-35)	71.3	✓	✓	✓	✓
SS	180	35	90	(20-35)	71.3	✓	✓	✓	✓
SS	195	35	90	(20-35)	71.3	✓	✓	✓	✓
SS	195	35	90	(20-35)	71.3	✓	✓	✓	✓
SS	210	35	90	(20-35)	71.3	✓	✓	✓	✓
SS	210	35	90	(20-35)	71.3	✓	✓	✓	✓
SS	225	35	90	(20-35)	71.3	✓	✓	✓	✓
SS	225	35	90	(20-35)	71.3	✓	✓	✓	✓
SS	240	35	90	(20-35)	71.3	✓	✓	✓	✓
SS	240	35	90	(20-35)	71.3	✓	✓	✓	✓
SS	270	35	90	(20-35)	71.3	✓	✓	✓	✓
SS	270	35	90	(20-35)	71.3	✓	✓	✓	✓
SS	300	35	90	(20-35)	71.3	✓	✓	✓	✓
SS	300	35	90	(20-35)	71.3	✓	✓	✓	✓
ES	10	5	85	(210-290)	49	×	×	×	×
ES	10	5	175	(210-290)	49	×	×	×	×
ES	20	69.2	103	(210-290)	49	×	×	×	×
ES	20	140	80	(210-290)	49	×	×	×	×
ES	30	235	40	(210-290)	49	✓	✓	✓	✓
ES	30	240	50	(210-290)	49	✓	✓	✓	✓
ES	40	231.2	40	(210-290)	49	✓	✓	✓	✓
ES	40	240	50	(210-290)	49	✓	✓	✓	✓
ES	50	205	36	(210-290)	49	✓	✓	✓	✓
ES	50	220	50	(210-290)	49	✓	✓	✓	✓
ES	60	220	50	(210-290)	49	✓	✓	✓	✓
ES	60	220	50	(210-290)	49	✓	✓	✓	✓
ES	75	220	50	(210-290)	49	✓	✓	✓	✓
ES	75	215	40	(210-290)	49	✓	✓	✓	✓
ES	90	240	50	(210-290)	49	✓	✓	✓	✓
ES	90	240	40	(210-290)	49	✓	✓	✓	✓
ES	105	240	50	(210-290)	49	✓	✓	✓	✓
ES	105	240	40	(210-290)	49	✓	✓	✓	✓
ES	120	235	50	(210-290)	49	✓	✓	✓	✓

ES	120	235	40	(210-290)	49	✓	✓	✓	✓
ES	135	235	50	(210-290)	49	✓	✓	✓	✓
ES	135	235	40	(210-290)	49	✓	✓	✓	✓
ES	150	235	50	(210-290)	49	✓	✓	✓	✓
ES	150	235	50	(210-290)	49	✓	✓	✓	✓
ES	165	235	50	(210-290)	49	✓	✓	✓	✓
ES	165	235	50	(210-290)	49	✓	✓	✓	✓
ES	180	220	50	(210-290)	49	✓	✓	✓	✓
ES	180	220	50	(210-290)	49	✓	✓	✓	✓
ES	195	235	50	(210-290)	49	✓	✓	✓	✓
ES	195	235	50	(210-290)	49	✓	✓	✓	✓
ES	210	235	50	(210-290)	49	✓	✓	✓	✓
ES	210	235	50	(210-290)	49	✓	✓	✓	✓
ES	225	240	50	(210-290)	49	✓	✓	✓	✓
ES	225	240	50	(210-290)	49	✓	✓	✓	✓
ES	240	240	50	(210-290)	49	✓	✓	✓	✓
ES	240	240	50	(210-290)	49	✓	✓	✓	✓
ES	270	240	50	(210-290)	49	✓	✓	✓	✓
ES	270	240	50	(210-290)	49	✓	✓	✓	✓
ES	300	240	50	(210-290)	49	✓	✓	✓	✓
ES	300	240	50	(210-290)	49	✓	✓	✓	✓
PA	10	33	84	(65-90)	153	×	×	×	×
PA	10	40	5	(65-90)	153	×	×	×	×
PA	20	65	140	(65-90)	153	✓	✓	✓	✓
PA	20	65	140	(65-90)	153	✓	✓	✓	✓
PA	30	67.5	155	(65-90)	153	✓	✓	✓	✓
PA	30	70	140	(65-90)	153	✓	✓	✓	✓
PA	40	35	30	(65-90)	153	×	×	×	×
PA	40	60	130	(65-90)	153	✓	✓	×	✓
PA	50	40	30	(65-90)	153	×	×	×	×
PA	50	75	140	(65-90)	153	✓	✓	✓	✓
PA	60	50	30	(65-90)	153	×	✓	×	×
PA	60	70	135	(65-90)	153	✓	✓	✓	✓
PA	75	83	94	(65-90)	153	✓	✓	×	×
PA	75	105	155	(65-90)	153	✓	✓	✓	✓
PA	90	100	150	(65-90)	153	✓	✓	✓	✓
PA	90	100	140	(65-90)	153	✓	✓	✓	✓
PA	105	90	90	(65-90)	153	✓	✓	×	×
PA	105	100	140	(65-90)	153	✓	✓	✓	✓
PA	120	100	145	(65-90)	153	✓	✓	✓	✓
PA	120	100	155	(65-90)	153	✓	✓	✓	✓
PA	135	100	145	(65-90)	153	✓	✓	✓	✓
PA	135	100	150	(65-90)	153	✓	✓	✓	✓
PA	150	107.5	145	(65-90)	153	✓	✓	✓	✓
PA	150	110	150	(65-90)	153	×	✓	✓	✓
PA	165	107.5	145	(65-90)	153	✓	✓	✓	✓
PA	165	110	140	(65-90)	153	×	✓	✓	✓
PA	180	105	150	(65-90)	153	✓	✓	✓	✓
PA	180	110	140	(65-90)	153	×	✓	✓	✓
PA	195	105	150	(65-90)	153	✓	✓	✓	✓

PA	195	110	140	(65-90)	153	×	✓	✓	✓
PA	210	88.8	95	(65-90)	153	✓	✓	×	×
PA	210	100	145	(65-90)	153	✓	✓	✓	✓
PA	225	60	90	(65-90)	153	✓	✓	×	×
PA	225	100	140	(65-90)	153	✓	✓	✓	✓
PA	240	82.5	115	(65-90)	153	✓	✓	×	×
PA	240	105	145	(65-90)	153	✓	✓	✓	✓
PA	270	105	140	(65-90)	153	✓	✓	✓	✓
PA	270	105	140	(65-90)	153	✓	✓	✓	✓
PA	300	105	140	(65-90)	153	✓	✓	✓	✓
PA	300	105	140	(65-90)	153	✓	✓	✓	✓
IO	10	5	85	(1200-1600)	149	×	×	×	×
IO	10	5	175	(1200-1600)	149	×	×	×	✓
IO	20	5	85	(1200-1600)	149	×	×	×	×
IO	20	5	175	(1200-1600)	149	×	×	×	✓
IO	30	5	85	(1200-1600)	149	×	×	×	×
IO	30	5	175	(1200-1600)	149	×	×	×	✓
IO	40	5	85	(1200-1600)	149	×	×	×	×
IO	40	5	175	(1200-1600)	149	×	×	×	✓
IO	50	257.5	105	(1200-1600)	149	×	×	×	×
IO	50	320	140	(1200-1600)	149	×	×	✓	✓
IO	60	257.5	105	(1200-1600)	149	×	×	×	×
IO	60	320	140	(1200-1600)	149	×	×	✓	✓
IO	75	257.5	105	(1200-1600)	149	×	×	×	×
IO	75	320	140	(1200-1600)	149	×	×	✓	✓
IO	90	725.5	118	(1200-1600)	149	×	×	×	×
IO	90	1080	160	(1200-1600)	149	✓	✓	✓	✓
IO	105	453.6	85	(1200-1600)	149	×	×	×	×
IO	105	705	150	(1200-1600)	149	×	×	✓	✓
IO	120	1075	150	(1200-1600)	149	✓	✓	✓	✓
IO	120	1095	160	(1200-1600)	149	✓	✓	✓	✓
IO	135	1053.3	103	(1200-1600)	149	✓	✓	×	×
IO	135	1080	160	(1200-1600)	149	✓	✓	✓	✓
IO	150	1053.3	103	(1200-1600)	149	✓	✓	×	×
IO	150	1080	160	(1200-1600)	149	✓	✓	✓	✓
IO	165	727.5	155	(1200-1600)	149	×	×	✓	✓
IO	165	735	150	(1200-1600)	149	×	×	✓	✓
IO	180	498	114	(1200-1600)	149	×	×	×	×
IO	180	720	150	(1200-1600)	149	×	×	✓	✓
IO	195	695	130	(1200-1600)	149	×	×	✓	✓
IO	195	720	150	(1200-1600)	149	×	×	✓	✓
IO	210	695	130	(1200-1600)	149	×	×	✓	✓
IO	210	720	150	(1200-1600)	149	×	×	✓	✓
IO	225	695	130	(1200-1600)	149	×	×	✓	✓
IO	225	700	160	(1200-1600)	149	×	×	✓	✓
IO	240	185	70	(1200-1600)	149	×	×	×	×
IO	240	700	160	(1200-1600)	149	×	×	✓	✓
IO	270	205	70	(1200-1600)	149	×	×	×	×
IO	270	700	160	(1200-1600)	149	×	×	✓	✓
IO	300	392	92	(1200-1600)	149	×	×	×	×

IO	300	700	160	(1200-1600)	149	×	×	✓	✓
AL	10	20	85	(54-65)	54	×	×	×	×
AL	10	20	175	(54-65)	54	×	×	×	×
AL	20	40	30	(54-65)	54	×	✓	×	✓
AL	20	45	160	(54-65)	54	✓	✓	×	×
AL	30	70	90	(54-65)	54	✓	✓	×	×
AL	30	70	90	(54-65)	54	✓	✓	×	×
AL	40	40	90	(54-65)	54	×	✓	×	×
AL	40	40	90	(54-65)	54	×	✓	×	×
AL	50	45	90	(54-65)	54	✓	✓	×	×
AL	50	65	23	(54-65)	54	✓	✓	×	×
AL	60	55	90	(54-65)	54	✓	✓	×	×
AL	60	85	40	(54-65)	54	×	✓	✓	✓
AL	75	60	75	(54-65)	54	✓	✓	×	✓
AL	75	85	40	(54-65)	54	×	✓	✓	✓
AL	90	60	70	(54-65)	54	✓	✓	✓	✓
AL	90	65	40	(54-65)	54	✓	✓	✓	✓
AL	105	65	70	(54-65)	54	✓	✓	✓	✓
AL	105	65	70	(54-65)	54	✓	✓	✓	✓
AL	120	60	70	(54-65)	54	✓	✓	✓	✓
AL	120	60	12	(54-65)	54	✓	✓	×	×
AL	135	65	70	(54-65)	54	✓	✓	✓	✓
AL	135	100	155	(54-65)	54	×	×	×	×
AL	150	68.3	83	(54-65)	54	✓	✓	×	✓
AL	150	90	150	(54-65)	54	×	×	×	×
AL	165	100	120	(54-65)	54	×	×	×	×
AL	165	105	145	(54-65)	54	×	×	×	×
AL	180	100	120	(54-65)	54	×	×	×	×
AL	180	100	135	(54-65)	54	×	×	×	×
AL	195	95	120	(54-65)	54	×	×	×	×
AL	195	95	130	(54-65)	54	×	×	×	×
AL	210	95	120	(54-65)	54	×	×	×	×
AL	210	100	150	(54-65)	54	×	×	×	×
AL	225	95	120	(54-65)	54	×	×	×	×
AL	225	100	150	(54-65)	54	×	×	×	×
AL	240	95	120	(54-65)	54	×	×	×	×
AL	240	100	150	(54-65)	54	×	×	×	×
AL	270	95	120	(54-65)	54	×	×	×	×
AL	270	100	140	(54-65)	54	×	×	×	×
AL	300	95	120	(54-65)	54	×	×	×	×
AL	300	100	140	(54-65)	54	×	×	×	×
GU	10	5	85	(40-60)	78	×	×	✓	✓
GU	10	5	175	(40-60)	78	×	×	×	×
GU	20	33.3	85	(40-60)	78	✓	✓	✓	✓
GU	20	50	65	(40-60)	78	✓	✓	✓	✓
GU	30	33.3	85	(40-60)	78	✓	✓	✓	✓
GU	30	50	65	(40-60)	78	✓	✓	✓	✓
GU	40	33.3	85	(40-60)	78	✓	✓	✓	✓
GU	40	50	65	(40-60)	78	✓	✓	✓	✓
GU	50	47.5	75	(40-60)	78	✓	✓	✓	✓

GU	50	50	60	(40-60)	78	✓	✓	✓	✓
GU	60	47.5	75	(40-60)	78	✓	✓	✓	✓
GU	60	50	60	(40-60)	78	✓	✓	✓	✓
GU	75	50	60	(40-60)	78	✓	✓	✓	✓
GU	75	50	60	(40-60)	78	✓	✓	✓	✓
GU	90	50	60	(40-60)	78	✓	✓	✓	✓
GU	90	50	60	(40-60)	78	✓	✓	✓	✓
GU	105	77.5	75	(40-60)	78	×	✓	✓	✓
GU	105	90	50	(40-60)	78	×	×	×	✓
GU	120	77.5	75	(40-60)	78	×	✓	✓	✓
GU	120	90	50	(40-60)	78	×	×	×	✓
GU	135	77.5	75	(40-60)	78	×	✓	✓	✓
GU	135	90	50	(40-60)	78	×	×	×	✓
GU	150	77.5	75	(40-60)	78	×	✓	✓	✓
GU	150	90	50	(40-60)	78	×	×	×	✓
GU	165	78.3	76	(40-60)	78	×	✓	✓	✓
GU	165	90	50	(40-60)	78	×	×	×	✓
GU	180	73	86	(40-60)	78	×	✓	✓	✓
GU	180	90	50	(40-60)	78	×	×	×	✓
GU	195	73	86	(40-60)	78	×	✓	✓	✓
GU	195	90	50	(40-60)	78	×	×	×	✓
GU	210	73	86	(40-60)	78	×	✓	✓	✓
GU	210	90	50	(40-60)	78	×	×	×	✓
GU	225	73	86	(40-60)	78	×	✓	✓	✓
GU	225	90	50	(40-60)	78	×	×	×	✓
GU	240	73	86	(40-60)	78	×	✓	✓	✓
GU	240	90	50	(40-60)	78	×	×	×	✓
GU	270	71.5	73	(40-60)	78	✓	✓	✓	✓
GU	270	90	50	(40-60)	78	×	×	×	✓
GU	300	75	45	(40-60)	78	×	✓	×	×
GU	300	75	90	(40-60)	78	×	✓	✓	✓
NI	10	5	85	(330-425)	150	×	×	×	×
NI	10	5	175	(330-425)	150	×	×	×	✓
NI	20	57.5	72	(330-425)	150	×	×	×	×
NI	20	70	0	(330-425)	150	×	×	×	×
NI	30	82	68	(330-425)	150	×	×	×	×
NI	30	160	140	(330-425)	150	×	×	✓	✓
NI	40	118.8	75	(330-425)	150	×	×	×	×
NI	40	220	140	(330-425)	150	×	×	✓	✓
NI	50	105	35	(330-425)	150	×	×	×	×
NI	50	250	140	(330-425)	150	×	✓	✓	✓
NI	60	170.8	56	(330-425)	150	×	×	×	×
NI	60	250	140	(330-425)	150	×	✓	✓	✓
NI	75	197.5	110	(330-425)	150	×	×	×	×
NI	75	250	140	(330-425)	150	×	✓	✓	✓
NI	90	247.5	150	(330-425)	150	×	✓	✓	✓
NI	90	245	150	(330-425)	150	×	✓	✓	✓
NI	105	250	140	(330-425)	150	×	✓	✓	✓
NI	105	245	150	(330-425)	150	×	✓	✓	✓
NI	120	237.5	130	(330-425)	150	×	✓	✓	✓

NI	120	250	140	(330-425)	150	×	✓	✓	✓
NI	135	238.3	148	(330-425)	150	×	✓	✓	✓
NI	135	250	140	(330-425)	150	×	✓	✓	✓
NI	150	260	160	(330-425)	150	×	✓	✓	✓
NI	150	260	140	(330-425)	150	×	✓	✓	✓
NI	165	255	156	(330-425)	150	×	✓	✓	✓
NI	165	260	140	(330-425)	150	×	✓	✓	✓
NI	180	228	156	(330-425)	150	×	✓	✓	✓
NI	180	235	140	(330-425)	150	×	✓	✓	✓
NI	195	228	156	(330-425)	150	×	✓	✓	✓
NI	195	235	140	(330-425)	150	×	✓	✓	✓
NI	210	224.3	131	(330-425)	150	×	×	✓	✓
NI	210	235	140	(330-425)	150	×	✓	✓	✓
NI	225	240	160	(330-425)	150	×	✓	✓	✓
NI	225	250	140	(330-425)	150	×	✓	✓	✓
NI	240	228.8	117	(330-425)	150	×	×	×	×
NI	240	250	140	(330-425)	150	×	✓	✓	✓
NI	270	160	0	(330-425)	150	×	×	×	×
NI	270	220	140	(330-425)	150	×	×	✓	✓
NI	300	180	106	(330-425)	150	×	×	×	×
NI	300	220	140	(330-425)	150	×	×	✓	✓
TO	10	5	85	(250-300)	21	×	×	×	×
TO	10	5	175	(250-300)	21	×	×	×	×
TO	20	197.5	62	(250-300)	21	×	✓	×	×
TO	20	225	20	(250-300)	21	✓	✓	✓	✓
TO	30	224.4	70	(250-300)	21	✓	✓	×	×
TO	30	265	40	(250-300)	21	✓	✓	✓	✓
TO	40	259	84	(250-300)	21	✓	✓	×	×
TO	40	290	40	(250-300)	21	✓	✓	✓	✓
TO	50	222.5	65	(250-300)	21	✓	✓	×	×
TO	50	325	50	(250-300)	21	✓	✓	×	✓
TO	60	295	20	(250-300)	21	✓	✓	✓	✓
TO	60	300	50	(250-300)	21	✓	✓	×	×
TO	75	295	20	(250-300)	21	✓	✓	✓	✓
TO	75	300	50	(250-300)	21	✓	✓	×	✓
TO	90	327.5	15	(250-300)	21	✓	✓	✓	✓
TO	90	330	10	(250-300)	21	✓	✓	✓	✓
TO	105	328.3	10	(250-300)	21	✓	✓	✓	✓
TO	105	310	50	(250-300)	21	✓	✓	✓	✓
TO	120	328.3	10	(250-300)	21	✓	✓	✓	✓
TO	120	330	50	(250-300)	21	✓	✓	✓	✓
TO	135	300	35	(250-300)	21	✓	✓	✓	✓
TO	135	320	10	(250-300)	21	✓	✓	✓	✓
TO	150	277.5	35	(250-300)	21	✓	✓	✓	✓
TO	150	320	10	(250-300)	21	✓	✓	✓	✓
TO	165	325	20	(250-300)	21	✓	✓	✓	✓
TO	165	330	10	(250-300)	21	✓	✓	✓	✓
TO	180	292	35	(250-300)	21	✓	✓	✓	✓
TO	180	330	10	(250-300)	21	✓	✓	✓	✓
TO	195	255	50	(250-300)	21	✓	✓	✓	✓

TO	195	325	20	(250-300)	21	✓	✓	✓	✓
TO	210	255	50	(250-300)	21	✓	✓	✓	✓
TO	210	310	20	(250-300)	21	✓	✓	✓	✓
TO	225	255	50	(250-300)	21	✓	✓	✓	✓
TO	225	310	20	(250-300)	21	✓	✓	✓	✓
TO	240	255	50	(250-300)	21	✓	✓	✓	✓
TO	240	310	20	(250-300)	21	✓	✓	✓	✓
TO	270	255	50	(250-300)	21	✓	✓	✓	✓
TO	270	310	20	(250-300)	21	✓	✓	✓	✓
TO	300	255	50	(250-300)	21	✓	✓	✓	✓
TO	300	310	20	(250-300)	21	✓	✓	✓	✓